BACHELOR'S THESIS / BIOMEDICAL ENGINEERING 2021

Alteration in nerve function following electroporation: a numerical modeling study of the electroporation conductance effect.

Sergi Marcoval i Martínez

upf. Universitat Pompeu Fabra Barcelona

Alteration in nerve function following electroporation:

A numerical modeling study of the electroporation conductance effect

Sergi Marcoval i Martínez

Bachelor's thesis UPF 2020/2021

Thesis supervisors:

Dr. Antoni Ivorra, DTIC

Dr. Tomás García-Sánchez, DTIC

Acknowledgments

I would like to express my sincere gratitude to my thesis supervisors Dr. Antoni Ivorra and Dr. Tomás García-Sánchez for the support, patience, motivation, enthusiasm, and immense knowledge.

I am extremely thankful to my family and friends for the continuous support in this effort.

Abstract

It is known that, after the application of sufficiently high external electric fields, defects are formed in the cell membrane at the molecular level, non-selectively increasing its permeability, and therefore increasing the conductance of the membrane to any ion. This phenomenon is called electroporation. Its effects may alter the excitable cell's ability to depolarize. Experimentally, it has been observed that conduction velocity in nerve fibers and contraction force in muscles are lowered after the delivery of high electric fields. This bachelor's thesis aims to develop a mechanistic model to assess whether it is plausible that those experimental observations are due to the direct effect of electroporation on the membrane. The cable model of an axon has been used to evaluate the effect of the increase of conductance due to electroporation on nerve fibers. The conductance increase has been modeled following two approaches at different level of detail: constant or dynamic. As hypothesized, the results suggest that the increase in membrane conductance due to electroporation may alter the function of nerve fibers, being able to reduce their conduction velocity, block completely the action potential propagation along them, and reduce their excitability. Moreover, in this bachelor's thesis, it is also shown for the first time that the blocking effect of kilohertz frequency alternating currents may be related to electroporation of nerve fibers. In this way, the model would be useful to predict whether a nerve fiber would be temporally "deactivated", given a certain distribution of the applied external voltage.

Keywords

Electroporation, nerve stimulation, nerve block, membrane conductance, electroporation conductance.

Prologue

This bachelor's thesis has been carried out in collaboration with the Biomedical Electronics Research Group (BERG), whose research is focused on bioelectrical phenomena and on exploring the use of these phenomena for developing new methods and devices for biomedical applications. In particular, it has been developed in the framework of different research grants related to electroporation. Namely, this thesis was developed with the support of the Beatriu de Pinós postdoctoral programme of the Government of Catalonia's Secretariat for Universities and Research of the Ministry of Economy and Knowledge in a research project related with the basis of the electroporation phenomenon. Additionally, two other research projects should be mentioned in the framework of this work: project PID2019-110120RB-I00/AEI/10.13039/501100011033 funded by the Ministry of Science, Innovation and Universities and the Spanish National Research (AEI) and a second project DTS20/00011 funded by the Instituto de Salud Carlos III (ISCIII) and FEDER both dealing with the use of irreversible electroporation in the treatment of cardiac arrhythmias.

Index

1. INTRODUCTION 1
1.1. Electroporation phenomenon 1
a) Overview 1
b) Pore formation and resealing 1
c) In vivo electroporation applications in medicine 2
1.2. Electrical stimulation of peripheral nerves 3
a) Overview 3
b) Excitable cells 3
c) Action potentials 4
d) Action potential propagation 5
e) The neuromuscular system 6
1.3. Experimental evidence of nerve block during and after electric field exposure 6
1.4. Hypotheses. 9
1.5. Objective. 9
2. METHODS 9
2.1. State of the art. Electroporation models. 9
2.2. Nerve Fiber Model. Cable model 11
2.3. Electroporation modeling 13
a) Constant electroporation conductance modeling 13
b) Dynamic electroporation conductance modeling. 15
c) KHFAC modeling 16
2.4. Conduction velocity ($\boldsymbol{CV}$) determination 16
3. RESULTS 17
3.1. Constant electroporation conductance 17
a) Blocking analysis 17
b) Excitability analysis 18
3.2. Dynamic electroporation conductance 19
a) Analysis of electroporation variables 19
b) Conduction block protocol 24
c) KHFAC modeling 26
4. DISCUSSION 29
5. CONCLUSION 30
BIBLIOGRAPHY 31
SUPPORTING INFORMATION 35
- SI-1. Equations describing the ionic currents 35
- References 37

List of figures

Page.

Figure 1. Molecular-level scheme of electroporation with the electric field perpendicular to the bilayer plane. **A**: the intact bilayer. **B**: water molecules start penetrating the bilayer, forming a water wire. **C**: the lipids adjacent to the water wire start reorientating toward the wire with their polar head groups, stabilizing the pore and allowing more water, as well as other polar molecules and ions, to enter. Adapted from [1]. 1

Figure 2. Transport of Na^+ and K^+ ions through ion channels. Conformational changes in protein molecules are also shown to open or close the "gates". Taken from [11]..... 4

Figure 3. Typical nerve action potential..... 5

Figure 4. Propagation of an action potential in both direction along a nerve fiber. Adapted from [11]..... 6

Figure 5. Motor unit. Taken from [2]..... 6

Figure 6. **A**: schematic of the cable model used to represent a nerve fiber. Adapted from [25]. **B**: illustration of a nerve fiber represented by the cable model presented in A. Adapted from [2]..... 11

Figure 7. Electrode configurations used in the study. **A. General scenario**: centered electrodes with a separation distance between them of 30 mm, and 10 mm from the nerve fiber. **B. Electroporation scenario:** centered electrodes with a separation distance between them of 5mm, and 2 mm from the nerve fiber. **C. Stimulation scenario**: electrodes in front of the distal nodes of the nerve fiber, with a separation distance between them of 5 mm, and 2 mm from the nerve fiber..... 13

Figure 8. Cable model considering the electroporation conductance. Adapted from [25]..... 13

Figure 9. **A:** blocking analysis scheme. **B:** excitability analysis scheme..... 14

Figure 10. Conduction velocity vs. electroporation conductance stimulating the right nodes with a 0.5 V monophasic pulse with a duration of 100 μs. G_e considered in nodes 38-48..... 17

Figure 11. ΔTMV along the nodes in each time step stimulating the right nodes with a 0.5 V monophasic pulse with a duration of 100 μs. G_e considered in nodes 38-48. **A**: without considering electroporation conductance ($G_e = 0$ S / m^2). **B:** considering G_e threshold ($G_e = 2379$ S / m^2). The red arrow indicates the block of the action potential propagation..... 18

Figure 12. G_e vs. stimulation threshold. Stimulating the nerve fiber through the general scenario with a monophasic pulse with a duration of 100 μs..... 18

Figure 13. Conduction velocity vs. electroporation conductance. Stimulating the nerve fiber through the general scenario with a 100 V monophasic pulse with a duration of 100 μs. G_e considered in all nodes..... 19

Figure 14 ΔTMV along the nodes in each time step. Stimulating the nerve fiber through a 100 V monophasic pulse with a duration of 100 μs. G_e in all nodes. **A**: without considering electroporation conductance ($G_e = 0$ S / m^2). **B**: considering G_e threshold ($G_e = 1275$ S / m^2)..... 19

Figure 15. g_e dependency on v_m..... 20

Figure 16. Time course of the ΔTMV at node 41 of the nerve fiber after stimulating the medial nodes with different strength voltages between the electrodes..... 20
Figure 17. Time course of g_e (**A**), N (**B**), G_e (**C**), and I_e (**D**) at node 41 of the nerve fiber stimulating the medial nodes with different strength voltages between the electrodes..... 21
Figure 18. Time course of ΔTMV (**A**), g_e (**B**), N (**C**), G_e (**D**), and I_e (**E**) at all nodes after stimulating the nerve fiber with a 100 V monophasic pulse with a duration of 100 μs in the general scenario..... 22
Figure 19. Time course of ΔTMV (**A**), g_e (**B**), N (**C**), G_e (**D**), and I_e (**E**) at all nodes after stimulating the nerve fiber with a 1000 V monophasic pulse with a duration of 100 μs in the general scenario..... 23
Figure 20. 1 ms time course of g_e (**A**), N (**B**), G_e (**C**), I_e (**D**), and ΔTMV (**E**) at node 41 after electroporating the middle nodes with a 15 V monophasic pulse with a duration of 100 μs vs. after electroporating with a 350 V monophasic pulse with a duration of 100 μs..... 24
Figure 21. Time course of ΔTMV at all nodes. (**A**) Stimulating the right nodes with a 0.5 V monophasic pulse with a duration of 100 μs after a previous electroporation of the nerve with a 15 V monophasic pulse with a duration of 100 μs (CV = 65.46 m / s). (**B**) Stimulating the right nodes with a 0.5 V monophasic pulse with a duration of 100 μs, without a previous electroporation of the nerve (CV = 65.67 m / s)..... 25
Figure 22. Time course of ΔTMV at all nodes. (**A**) Stimulating the right nodes with a 0.5 V monophasic pulse with a duration of 100 μs after a previous electroporation of the nerve with a 350 V monophasic pulse with a duration of 100 μs (CV = 0 m / s). (**B**) Stimulating the right nodes with a 0.5 V monophasic pulse with a duration of 100 μs, without a previous electroporation of the nerve (CV = 65.67 m / s)..... 26
Figure 23. Time course of g_e (**A**), N (**B**), G_e (**C**), I_e (**D**), and ΔTMV (**E**) at node 41 when electroporating with a KHFAC sine wave of 3 kHz with an amplitude of 10 V_{pp}…….. 27
Figure 24. Zoom in the time course of g_e (**A**), N (**B**), G_e (**C**), I_e (**D**), and ΔTMV (**E**) at node 41 when electroporating with a KHFAC sine wave of 3 kHz with an amplitude of 10 V_{pp}..... 27
Figure 25. **A**: time course of G_e at node 41 when electroporating with a KHFAC sine wave of 3 kHz with an amplitude of 15 V_{pp}. **B**: zoom in the time course of G_e at node 41 when electroporating with a KHFAC sine wave of 3 kHz with an amplitude of 15 V_{pp}…… 28

List of tables

Page

Table 1. Experimental evidence on how electric field exposure can affect nerve fiber function..... 7
Table 2. Summary of electroporation modeling studies..... 10
Table 3. Parameters used in the cable model..... 12
Table 4. Electroporation parameters..... 15

1. INTRODUCTION

1.1. Electroporation phenomenon

a) Overview

Electroporation is the increase in the permeability of the cell membrane due to externally applied electric fields. Currently, there is a broad consensus that the electroporation phenomenon is best described, at least during its initial stages, as the formation of aqueous pores in the lipid bilayer. Aqueous pore formation is initiated by the penetration of water molecules into the bilayer of the membrane, leading to the reorientation of adjacent lipids with their polar head groups pointing toward these water molecules. Unstable pores with nanosecond lifetimes can spontaneously form even in the absence of an external electric field, but exposure of the membrane to an electric field reduces the energy required for penetration of water into the bilayer. In the first nanoseconds, the penetration is mainly caused by the transfer of the external field to the membrane, and then, within a microsecond, the transmembrane field is amplified by polarization, resulting in the increase of an induced transmembrane voltage (TMV). The entrance of water increases the probability of pore formation, resulting in a greater number of more stable pores formed in the membrane per unit of area [1] (see Figure 1).

Electroporation is usually induced by exposing cells to short (from a few nanoseconds to a few milliseconds) high intensity electric fields pulses to avoid thermal damage to the cellular structures due to Joule heating [2].

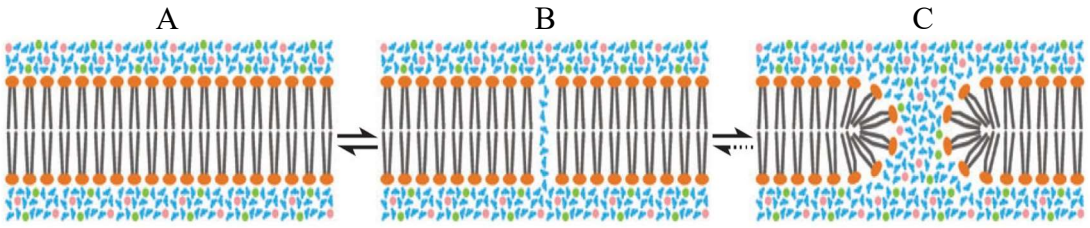

*Figure 1. Molecular-level scheme of electroporation with the electric field perpendicular to the bilayer plane. **A**: the intact bilayer. **B**: water molecules start penetrating the bilayer, forming a water wire. **C**: the lipids adjacent to the water wire start reorientating toward the wire with their polar head groups, stabilizing the pore and allowing more water, as well as other polar molecules and ions, to enter. Adapted from [1].*

b) Pore formation and resealing

Depending on the characteristics of the applied electric field (magnitude, duration, number of applications, and application repetition frequency), cell size, cell population, and cell orientation with respect to the electric field direction, the molecular effect upon the cellular membrane may be [1]:

1. **No detectable electroporation.** No detectable increase of molecular transport.
2. **Reversible electroporation.** Temporary and limited pores are formed in the cell membrane for molecular transport, but once the electrical pulse ends, transport begins to cease, and cells remain viable. This cessation of transport is due to the pore resealing, in which the membrane conductivity returns to its preporation value. This process is often completed within seconds, or even minutes, after the end of the exposure.
3. **Nonthermal irreversible electroporation (NTIRE).** This term refers to cell death caused by electroporation. Cell death due to electroporation can be either caused by the inability of the cells to reseal the pores, leading to short-term cell death, or by excessive homeostasis alteration, even when the cells are able of finally restoring their membranes, leading to death in later periods. This cell death after electroporation may be caused by the loss of metabolites, generation of reactive oxygen species, damage or modification of cytoskeleton function, or initiation of secondary processes [1][3].
4. **Irreversible electroporation accompanied by thermal effects**. The electric currents cause a temperature increase sufficiently high to thermally damage the cell.

c) In vivo electroporation applications in medicine

Currently, there are various applications of in vivo electroporation in medical practice:

1. **Electrochemotherapy.** Cell electroporation for delivery of non- or poorly permeant chemotherapeutic drugs (e.g. bleomycin), which allows their transmembrane transport to increase their cytotoxicity [1].
2. **Gene therapy.** Gene electrotransfer to cells and tissues for gene therapy (e.g. for cancer treatment in melanomas [4] or prostate cancer [5], among others), and DNA vaccination (against infectious diseases and regenerative therapy [1]).
3. **NTIRE.** Emerging minimally invasive surgical procedure for tissue ablation, in which pulsed electric fields are externally applied to cause irreversible damage to cells, without affecting the tissue scaffold, large blood vessels, and other tissue structures [6]. In clinics, tissue is ablated by externally applying a series of short and intense square electric pulses through electrodes inserted directly into, or placed around, the target tissue. Monophasic 100 μs pulses are the most used ones [7]. This procedure is used to destroy tumors [8] and to treat other non-cancerous pathologies, such as atrial fibrillation [9].

These electroporation-based treatments are accompanied by muscle contractions and acute pain as a side effect, causing discomfort to patients and potential clinical complications. First, to overcome acute pain, it is necessary to administer local or general anesthesia. Second, muscle contractions may displace the electrodes and change the outcome of the treatment by changing the distribution of the electric fields that are applied with respect to the prior planning. Finally, such electrode displacement may mechanically damage vital structures close to the region being treated. Thus, sometimes it is necessary to administer paralytic agents [7][10].

1.2. Electrical stimulation of peripheral nerves

a) Overview

Peripheral nerves are the structures that connect the central nervus system (CNS) with peripheral organs or muscles, through the peripheral nervous system (PNS). This connection allows the body to carry out many functions [2]:

1. Information from the sensory receptors is transmitted to the CNS and can be transduced into sensations.
2. The connection with the CNS allows regulation of the skeletal muscle contractions, which enables controlled movement of the body.
3. Communication between the CNS and the smooth muscles allows the CNS to interfere with the functioning of the organs.
4. The CNS can control some glands of the body by regulating their secretion [11].

This transmission of information is based on the conduction of so-called *action potentials* (APs), which can be considered to be electric signals and were historically labeled *nerve impulses*, along the nerves. This process is explained in the next subsections.

b) Excitable cells

Excitable cells (e.g. neurons and muscle cells) are those cells that can generate and propagate action potentials. In this subsection, the cell membrane is briefly described first, and then, it is presented how some elements of the cell membrane makes possible the excitability of these cells.

In cell membranes, the lipid bilayer is not miscible with either the extracellular fluid or the intracellular fluid. Thus, it constitutes a barrier against the movement of water molecules and water-soluble substances between the extracellular and intracellular fluid compartments. In the cell membrane there are protein molecules with different properties for transporting substances, and they play a key role in maintaining the cell homeostasis. Among these proteins, ion channels are complex structures that can change its conformation allowing diffusion of ions across the cell membrane. These ions can be highly selective for the ion type, or they can allow any ion to diffuse, and their activation or inactivation (opening and closing) can be driven by different stimulus (electrical, chemical, or mechanical) [2][7][11]. In these ion channels, transport is completely passive, which means that it is only driven by concentration gradient between the intracellular and the extracellular space. On the other hand, there are other proteins (ion pumps) in the lipid bilayer that involve the active transport ions and allow the exchange of ions against the concentration gradient [2].

Both ion channels and ion pumps play an important role in excitable cells function. On the one hand, some ion channels are activated in a TMV-dependent manner (called voltage-gated ion channels) and give excitable cells the ability to generate and propagate action potentials, making them also excitable by external electrical stimuli [2][7]. On the other hand, ion pumps restore the initial concentration gradient between the extracellular and intracellular fluids, after the generation of the action potential [11].

c) Action potentials

Action potentials are rapid perturbations of the transmembrane voltage that can propagate. In this process, Na^+ and K^+ ions play an important role as well as their associated voltage-gated ions channels (Figure 2).

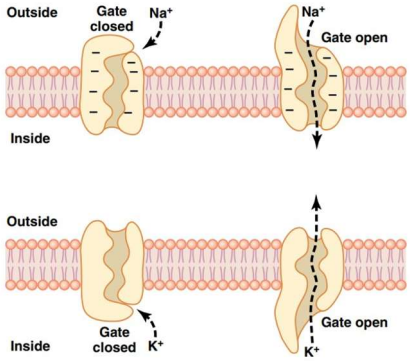

Figure 2. Transport of Na^+ and K^+ ions through ion channels. Conformational changes in protein molecules are also shown to open or close the "gates". Taken from [11]

APs are triggered when there is a depolarization that increases the TMV above a certain threshold. This momentary change in TMV is caused by changes in the ion concentration across the membrane and is mediated by the previously mentioned ionic channels. This depolarization can be triggered by an external stimulus, or by the depolarization of a nearby patch of membrane. Figure 3 shows the TMV changes that occur during an action potential, with the transfer of positive charges to the interior of the fiber at its onset (depolarization) and return of positive charges to the exterior at its end (repolarization) [11]. The stages of an action potential are [2]:

- **Resting stage.** There is an absence of alteration or stimulus. Therefore, excitable cell has a constant TMV (resting voltage), which depends on the intracellular and extracellular ionic concentrations, as well as their permeabilities through the membrane.
- **Depolarization stage.** Once the membrane is depolarized above a threshold, an action potential is triggered, and the membrane permeability to Na^+ increases rapidly (opening of the sodium channels), allowing a large number of Na^+ ions to enter the cell. This process generates a positive feedback effect: the entry of Na^+ raises the TMV, and at the same time, an increase in the TMV causes more Na^+ channels to open, thus increasing the influx even more.
- **Repolarization stage.** Once the TMV reaches the peak of the action potential, Na^+ channels begin to close while, at the same time, K^+ channels (which need a larger time to open) are still opening. Therefore, the positive feedback of the depolarization stage is stopped and there is an efflux of K^+ ions to the extracellular medium that causes a decrease in the TMV, returning it to the initial resting potential.
- **Refractory period stage**. After an action potential, there is a stage in which it is impossible to generate an action potential (absolute refractory period), and it is

followed by a period in which a greater than usual stimulus is required to generate an action potential (relative refractory period).

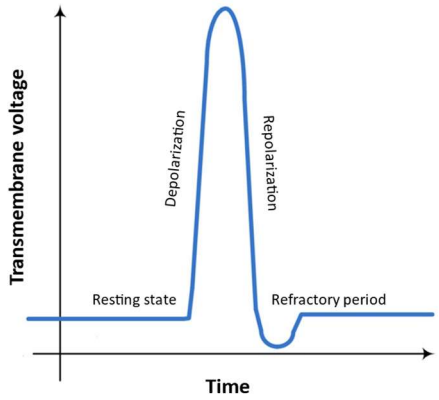

Figure 3. Typical nerve action potential

d) Action potential propagation

In the PNS, information is transmitted by propagating APs through the axons of neurons that are contained in the nerves. APs triggered at any one point on an excitable membrane usually excites adjacent portions of the membrane, resulting in its propagation along the membrane. Figure 4 (A) shows a normal resting nerve fiber (i.e. an axon), and Figure 4 (B) shows a nerve fiber that has been excited in its middle portion, and therefore, this portion suddenly develops a higher permeability to Na^+ ions [11].

The red arrows in Figure 4 (B) show a "local circuit" of current flow from the depolarized areas of the membrane to the adjacent areas of the membrane at rest. An excitable membrane does not have a single direction of propagation, the action potential travels in all directions away from the stimulus, until the entire membrane depolarizes. Normally, however, an AP is initiated at the terminus of the axon and propagates only in one direction [11].

This process is governed by the all-or-nothing principle: once an action potential has been elicited at any point in the membrane of a fiber, the depolarization process travels over the entire membrane if conditions are right, or does not travel at all if conditions are not right (if it does not generate enough voltage to stimulate the next patch of the membrane) [11].

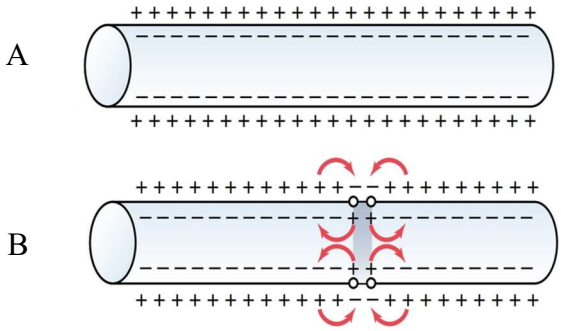

Figure 4. Propagation of an action potential in both direction along a nerve fiber. Adapted from [11]

e) The neuromuscular system

Muscles are controlled by the CNS through the motor neurons of the PNS. Muscle fibers are the contractile elements of the muscle, and the number of contractile fibers in the muscle depends on the size of the muscle. Muscle contractions are the result of the contraction of several muscle fibers, and its strength depends on the number of contracting fibers, as well as their individual strengths [2].

When an action potential reaches the axon terminal of a motor neuron, a neurotransmitter is released causing the depolarization of the muscle fiber. Then, a complex mechanism takes place producing a contraction [11]. One motor neuron can be connected to many muscle fibers (not the other way around), and the group of muscle fibers innervated by the motor neuron is called motor unit (MU) (see Figure 5), which is the smallest functional structure of the muscle that can be controlled by the CNS. Besides, the diameter of a motor neuron is related to the MU size (number of muscle fibers that contains) [12], and the number of muscle fibers in a MU varies largely between muscles and within MUs in the same muscle [2].

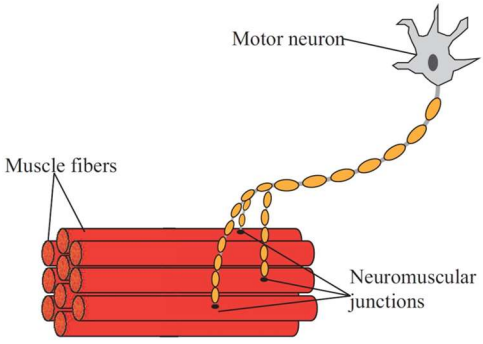

Figure 5. Motor unit. Taken from [2]

1.3. Experimental evidence of nerve block during and after electric field exposure

For years, several studies have revealed alterations in nerve function during and after exposure to external electric fields. Some of these studies, their protocols, the parameters they evaluated, and their experimental evidence are summarized in Table 1.

Table 1. Experimental evidence on how electric field exposure can affect nerve fiber function.

Study	Protocol	Parameter evaluated	Experimental observations
G.S. Abramov et. al., 1996 [13]	Twelve 4 ms electric field pulses of. 37 V / cm, 75 V/cm, and 150 V / cm with a 10 s interval between shocks were applied directly to the sciatic nerve of rats.	Conduction velocity	• 3 h postshock, the 37 V / cm group did not exhibit a nerve conduction velocity that were different from the preshock values, while in the other conditions they did. • Nerve conduction velocity following the 3 h recovery period appeared to have returned to the preshock values in the 37 and 75 V / cm groups but remained decreased in the 150 V / cm group. • Electroporation was suggested as an explanation.
H. Gissel et. al., 2002 [14]	Isolated and intact rat extensor digitorum longus muscles were exposed to electroporation paradigms (three 200 μs duration pulses at 313 V / cm and 500 V / cm at a frequency of 1 Hz.	Muscle force	• The 500 V / cm group induced a complete and lasting loss of force. • The 313 V / cm group resulted in an almost complete loss of force in the first 10 min. Subsequently, the force underwent a slow recovery and reached 85 % of the control level after 50 min. • Electroporation was suggested as an explanation.
T. Clausen et. al., 2005 [15]	Isolated and intact rat soleus muscles were exposed to electroporation paradigms (eight square waves pulses of 0.1 ms) in the range 100-800 V / cm, applied at a frequency of 1 Hz.	Muscle force	• At 100 V / cm, there was no reduction in force. • Pulses of 300 V / cm or more gave a prompt and complete loss of forces. • After pulses of 300 V/cm, about 80 % force recovery was obtained within 30-50 min. • At higher voltages, recovery was much slower and incomplete. • After pulses of 800 V/cm, only 3% force recovery was observed, even after 4 h. • Electroporation was suggested as an explanation.
Kilgore et. al., 2004 [16]	Two separated electrodes (stimulator, and blocking) were placed in the sciatic nerve of adult bullfrogs. Constant current stimuli at 10 μA for 200 μs with a	Muscle force	• 100 % of block was achieved throughout the period of block. • The nerve can conduct action potentials again from approximately 500 ms after cessation of block.

	frequency of 0.2 Hz was delivered through course of trial, and a KHFAC block consisting of 3 kHz sinusoidal waveform with amplitude of 10 V_{pp} was delivered from 10 s to 50 s of the trial.		• Electroporation was not suggested as an explanation.
Bhadra et. al., 2005 [17]	Two separated electrodes (stimulator, and blocking) were placed on the sciatic nerve of adult rats. Constant-current 100 μs stimuli was performed at 2 mA with a repetition frequency of 1 Hz. Parallelly, from 4 to 24 s after the first stimulation, a 18 kHz and 8 V (KHFAC) sinusoidal wave was delivered through the blocking electrode.	Muscle force	• Conduction block was produced immediately after the KHFAC delivery. • Within 1 s of the cessation of KHFAC wave, the muscle returns to pre-block force levels. • Electroporation was not suggested as an explanation.

G.S. Abramov et. al., 1996 [13] evaluated the conduction velocity (the velocity at which APs travel in a nerve fiber) of sciatic nerves in rats after exposure to pulsed electric fields of different magnitudes. They reported that after the electric field application, conduction velocity can be highly reduced. This reduction is higher for electric fields of greater magnitude. After a recovery period, they noticed that in the conditions with lower magnitude of the applied electric field, the nerve presented conduction velocities around the preshock values.

Other studies (H. Gissel et. al., 2002 [14], and T. Clausen et. al. 2005 [15]) with equivalent field exposure protocols, showed similar reductions and blockings in muscle contractile force. They noticed that these reductions are higher for electric fields of greater magnitude, and in the conditions with the lowest applied electric field, muscles can recover their initial force within a few minutes.

Besides, some studies (Kilgore et. al., 2004 [16], and Bhadra et. al, 2005 [17]) report instantaneous conduction block in nerve fibers by applying them low voltage and high-duration kilohertz frequency alternating current (KHFAC). This block has been shown to be fully and rapidly reversible.

These experimental observations could be explained as being the consequence of a direct effect of electroporation on the cell membrane conductance. And, indeed, such hypothesis has been indicated in [13][14][15]. Regarding to the KHFAC block, despite being low voltage electrical waveforms, they are applied for many seconds, potentially being able to cause a significant electroporation effect. To the best of our knowledge, the mechanism of action of KHFAC has never been related to electroporation; some authors hypothesize that mechanism of action of KHFAC is related to depolarization (inactivation of Na^+ channels) but the exact mechanism has not yet been demonstrated [17].

Besides of the experimental results discussed above, other studies have demonstrated the ability of short infrared laser pulses in reversible blocking APs in neurons [18][19]. In these studies, the observed conduction block could also be attributed to an increase in membrane permeability caused by laser exposure, followed by the membrane resealing. These studies support the idea that temporary changes in the permeability of the membrane can be responsible for changes in their ability to conduct APs.

1.4. Hypotheses.

The aqueous pores formed in the cell membranes after the application of external electric fields non-selectively increase the membrane permeability, and therefore, they also increase the conductance of the membrane to any ion (electroporation conductance). In this "permeable" state, the accumulation of charges in both sides of the membrane (external and internal) would be more difficult, decreasing the ability of excitable cells to generate APs.

In this way, electroporation would alter the functionality of nerve fibers in different ways:

1. Reducing their ability to propagate APs.
2. Blocking the AP propagation.
3. Reducing their excitability

1.5. Objective.

The general goal of this bachelor's thesis is to numerically study the plausibility of the above hypotheses. More specifically the aim of this bachelor's thesis is to develop a mechanistic model to assess whether the reduction of the conduction velocity in nerve fibers, and the reduction of muscle force after the external application of electric fields, observed in some experiments with pulsed fields of large magnitude [13][14][15] (see Table 1), can be explained as being the consequence of the primary effect of electroporation on the cell membrane (i.e. pore formation and therefore, the increment of the membrane conductance to any ion). In the same direction, it is intended for the first time to demonstrate whether the KHFAC conduction block observed in [16][17] (see Table 1) is also due to the effects of electroporation on the membrane.

2. METHODS

2.1. State of the art. Electroporation models.

For years, different studies have modeled the electroporation phenomenon at cellular level. The description of some of these models, and the parameters considered are summarized in Table 2. These studies have been evaluated to determine which would fit more in the context of the present study (one dimensional model of a nerve fiber).

Table 2. Summary of electroporation modeling studies.

Study	Description	Parameters considered
W. Krassowska, 1995 [20]	One-dimensional model of cardiac strand to investigate the effects of electroporation on transmembrane potential induced by defibrillation shocks.	Membrane conductance due to electroporation
DeBruin & Krassowska, 1997 [21]	One-dimensional fiber model to investigate the effects of electroporation and membrane kinetics on the transmembrane potential in a cardiac fiber.	Electroporation current, conductance of a single pore, number of pores per unit area.
K. Ohuchi et. al., 2002 [22]	A small pore description which mimics the reversible breakdown of the cell membrane incorporated into a model of a ventricular action potential, to elucidate the subcellular mechanism underlying the aftereffects of high intensity dc shocks.	Ionic currents and ion fluxes through a pore.
R. P. Joshi et. al., 2007 [23]	Numerical studies modifying the cable model to take account of the increased membrane conductance and the altered membrane capacitance during the application of high-intensity electric pulses.	Increased membrane conductance
J. Langus et. al., 2016 [24]	Time-dependent numerical model that provide an accurate prediction of the established electric current in the tissue throughout the whole duration of applied electric pulses during electroporation.	Tissue conductivity (depends on the level of poration, poration damage, and thermal damage indicators)

First, W. Krassowska, 1995 [20] has a direct implementation, but it only simulates the membrane conductance during the shock delivery. Therefore, the resealing after the shock delivery is not evaluated. Second, J. Langus et. al., 2016 [24] characterizes the resealing dynamics due to the electroporation after several pulses, but in a beef liver tissue, not in a one-dimensional strand. Third, K. Ohuchi, et. al., 2002 [22]. models the influence of the resealing on the action potential aftereffects when several pulses are applied in a cardiac cell. However, it is based on a description of ionic currents not compatible with the model used in the present study (see section 2.2. Nerve Fiber Model. Cable model). On the other hand, Joshi et. al. 2007 [23], modifies the cable model (see section 2.2. Nerve Fiber Model. Cable model) to take account of the increased membrane conductance and the altered membrane capacitance during the application of high-intensity electric pulses. Nevertheless, it considers tridimensional distributed electrical calculations, and therefore, the computational cost becomes too expensive.

Finally, DeBruin & Krassowska, 1997 [21] developed a model that best fits in the context of the present study, since it describes the electroporation effects and the membrane kinetics for a one-dimensional fiber. In addition, it considers different variables involved in the electroporation phenomenon: electroporation current, conductance of a single pore, and number of pores per unit area.

2.2. Nerve Fiber Model. Cable model

For assessing the response of a nerve fiber to a temporally applied external voltage, a one-dimensional cable model for myelinated nerve fibers (McNeal et.al., 1976 [25]) is used. The practical implementation of this model was developed by Borja Mercadal in the context of his PhD developed in BERG at Universitat Pompeu Fabra (see [2][7]) and it is used as basis for the present study.

In this model, a nerve fiber (i.e. axon) is discretized in n nodes of Ranvier (in the present study, n = 86), and the individual nodes are represented as circuit elements consisting of capacitance (C_m), membrane resistance (R_m), and a potential source (E_r), which maintains the transmembrane resting potential. The voltages $V_{e,n}$ are the extracellular nodal voltages, and they are the driving forces for changes in the membrane potential (see Figure 6). Between two nodes, $R_a$represents the longitudinal resistance of the axon.

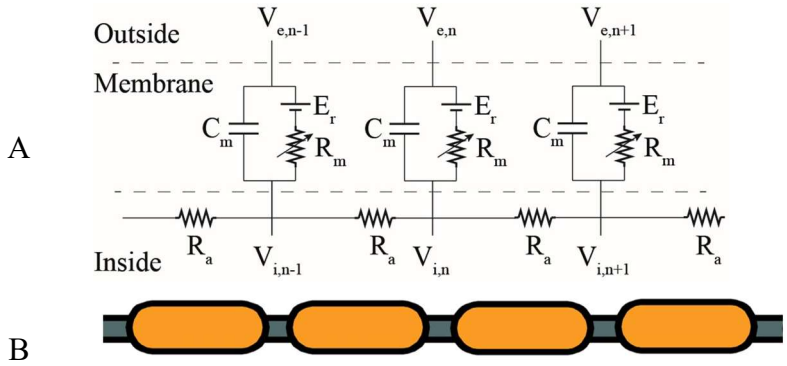

*Figure 6. **A**: schematic of the cable model used to represent a nerve fiber. Adapted from [25]. **B**: illustration of a nerve fiber represented by the cable model presented in A. Adapted from [2]*

Following this approach, the TMV relative to the resting voltage ($V_n = V_{i,n} - V_{e,n} - V_r$), at the nth node of Ranvier can be calculated by solving the equation:

$$\frac{dV_n}{dt} = \frac{1}{C_m}\left[G_a\left(V_{n-1} - 2V_n + V_{n+1} + V_{e,n-1} - 2V_{e,n} + V_{e,n+1}\right) - I_{i,n}\right] \qquad (1)$$

where $G_a$is the axonal conductance ($= 1/R_a$), and $I_{i,n}$is the ionic current across the membrane at each node. The ionic current is approximated as the sum of the current through 3 types of voltage gated ionic channels plus a leakage current as in [26] (see section SI-1. Equations describing the ionic currents). Assuming that no axial current can exit at the end of the fiber (sealed end assumption) [27], the voltage at the extreme nodes is calculated as:

$$\frac{dV_1}{dt} = \frac{1}{C_m}\left[G_a\left(-V_1 + V_2 - V_{e,1} + V_{e,2}\right) - I_{i,1}\right] \qquad (2)$$

$$\frac{dV_N}{dt} = \frac{1}{C_m}\left[G_a\left(-V_N + V_{N-1} - V_{e,N} + V_{e,N-1}\right) - I_{i,N}\right] \qquad (3)$$

Eq (1), (2) and (3) and the equations describing the evolution of the ionic currents are integrated by the implicit backward Euler method in *Matlab R2020b*. The parameters used in the model are listed in Table 3.

Table 3. Parameters used in the cable model.

Symbol	Value	Definition, justification, or source
ρ_a	$70\ \Omega \cdot \mathrm{cm}$	Axoplasmic resistivity [28]
c_m	$2\ \mu\mathrm{F/cm^2}$	Nodal capacitance [29]
L	$115 \cdot \mathrm{D}\ \mu\mathrm{m}$	Internodal distance [30][31]
G	$1\ \mu\mathrm{m}$	Nodal length [32]
D	$10\ \mu\mathrm{m}$	Fiber diameter
d_a	$0.7 \cdot \mathrm{D}\ \mu\mathrm{m}$	Axon diameter [32]
d_n	$0.33 \cdot \mathrm{D}\ \mu\mathrm{m}$	Node diameter [32]
C_m	$\mathrm{c_m}\pi d_n G$	Membrane capacity
G_a	$\frac{\pi d_a^2}{4\rho_a L}$	Axonal conductance
V_{rest}	$-80\ mV$	Resting voltage

In the present study, the extracellular voltages $V_{e,n}$ are obtained approximating the electric potential distribution in tissue generated by two ideal sphere electrodes (dipoles with opposite sign but equal strength) with a voltage difference between them, considering a uniform conducting medium of infinite extent:

$$V_{e,n} = \frac{\Delta V * r}{2}\left(\frac{1}{r_{+,n}} - \frac{1}{r_{-.n}}\right) \qquad (4)$$

Where ΔV is the voltage between the sphere electrodes, r (= 0.5 mm) is radius of the sphere electrodes, $r_{+,n}$ is the distance of each node to the anode, and $r_{-,n}$ is the distance of each node to the cathode. Note that for this aproximation, r must be much smaller than the separation distance between the electrodes.

The external voltage is calculated for three different electrode position scenarios, and are used depending on the case study. Figure 7 (A) shows the **general scenario**, in which the nerve fiber is stimulated by two centered electrodes with a separation distance between them of 30 mm, and 10 mm from the nerve fiber. Figure 7 (B) shows the **electroporation scenario**, in which the middle nodes of the nerve fiber are exposed to an electric field by two centered electrodes with a separation distance between them of 5 mm, and 2 mm from the nerve fiber. Finally, Figure 7 (C) shows the **stimulation scenario**, in which the right (distal) nodes of the nerve fiber are stimulated with two electrodes with a separation distance between them of 5 mm, and 2 mm from the nerve fiber. Different voltage amplitudes are studied for the different electrode position.

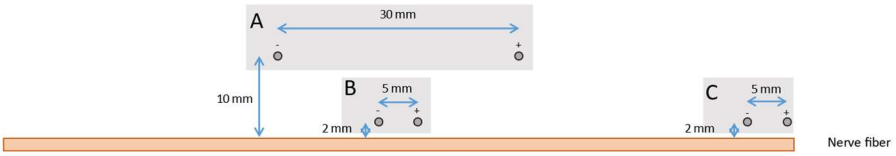

*Figure 7. Electrode configurations used in the study. **A. General scenario**: centered electrodes with a separation distance between them of 30 mm, and 10 mm from the nerve fiber. **B. Electroporation scenario:** centered electrodes with a separation distance between them of 5mm, and 2 mm from the nerve fiber. **C. Stimulation scenario**: electrodes in front of the distal nodes of the nerve fiber, with a separation distance between them of 5 mm, and 2 mm from the nerve fiber.*

Note that the external voltage is always applied 0.1 ms after the simulation begins, to assess the dynamics of the nerve fibers at rest.

2.3. Electroporation modeling

To consider the electroporation phenomenon in the cable model, a new additional conductance (electroporation conductance) is added in parallel to the membrane capacitance in each node, assuming that the electroporation only changes the conductance of the lipid bilayer. The representation of the cable model considering the electroporation conductance is presented in Figure 8, where G_e corresponds to the electroporation conductance.

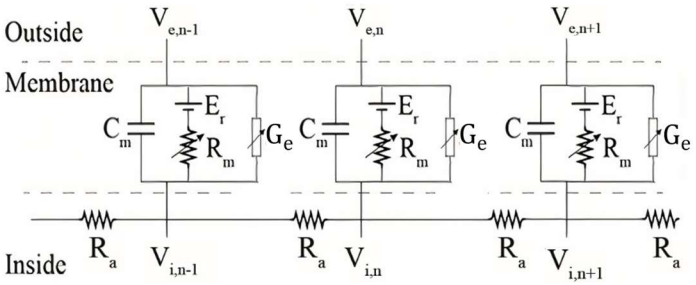

Figure 8. Cable model considering the electroporation conductance. Adapted from [25]

In the next subsections, two different ways in which G_e is modeled are explained.

a) Constant electroporation conductance modeling

First, the electroporation conductance is approximated with a constant behavior (ohmic) not taking into account any pore opening dynamics or resealing processes, in order to preliminary assess its impact on the nerve fiber function. In this way, G_e is modeled through a linear current (electroporation current, I_e), and its expression becomes:

$$I_e = G_e(V_m - E_e) \qquad (5)$$

where V_m is the transmembrane potential and $E_e$is the membrane Nerst potential (-90 mV).

First, it is evaluated how electroporation can impact on the AP propagation along the nerve fiber (**blocking analysis**). Subsequently, its impact on cell's excitability is assessed (**excitability analysis**).

The **blocking analysis** is carried out by modeling electroporation with constant values of G_e only in the 11 middle nodes of the nerve fiber (38-48), trying to reproduce a situation where only the central part of the fiber has been electroporated. Then, the conduction velocity between nodes 10 and 60 is calculated after stimulating with a 0.5 V monophasic pulse with a duration of 100 μs[1] the right nodes of the fiber. Besides, it is assessed the G_e threshold[2] (i.e. G_e minimum at which the action potential propagation is somehow blocked) (see Figure 9 (A)).

On the other hand, the **excitability analysis** is performed by adding G_e in all nodes (1-86) to assess how the stimulation threshold of the fiber (i.e. the minimum voltage at the electrodes that triggers an action potential at any node of the fiber) is modified for different values of G_e. In this case, electrode position corresponds to the general scenario (see Figure 7) considering 100 μs monophasic pulses. In this context, a blocking analysis is also carried out, calculating the conduction velocity between nodes 4 and 20, and applying a 100 V monophasic pulse with a duration of 100 μs (see Figure 9 (B)).

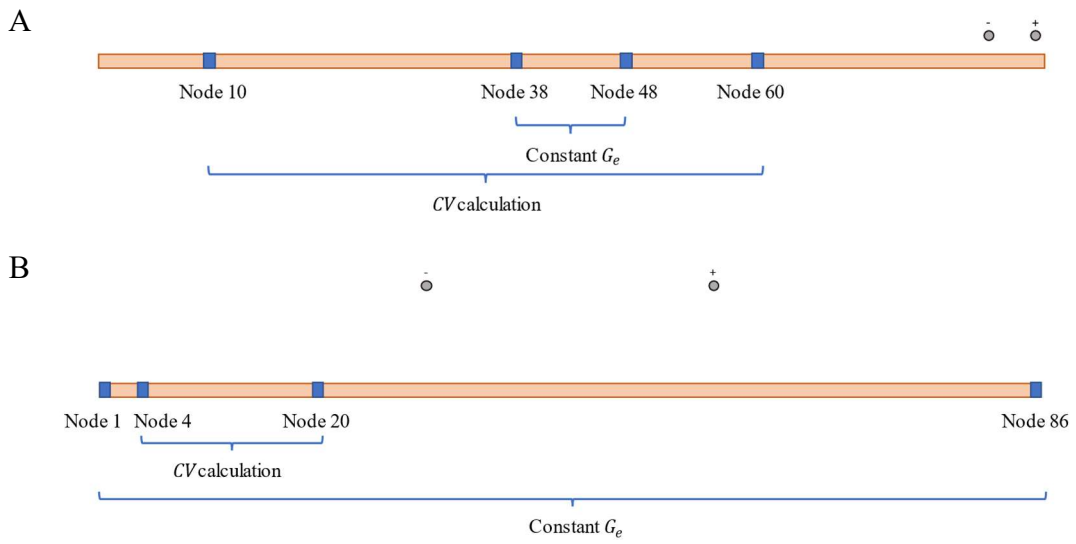

*Figure 9. **A:** blocking analysis scheme. **B:** excitability analysis scheme*

Nevertheless, this modeling does not represent the actual dynamics of G_e, since it is not actually ohmic, as it depends on different parameters (e.g. intensity of the applied external electric field, pore density…). In the next subsection, G_e is modeled considering some of these parameters, causing I_e to become non-linear.

[1] This stimulation is higher but close the stimulation threshold (i.e. the minimum voltage at the electrodes that triggers an action potential at any node of the fiber) when electroporation conductance is not considered in the model.

[2] The G_e threshold values are calculated with a resolution of 1 S / m^2

b) Dynamic electroporation conductance modeling.

The dynamic electroporation conductance is modeled as described Debruin & Krassowska, 1997 [21], and therefore, the I_e component becomes now to be the movement of ions through the shock-induced pores:

$$I_e = g_e * N * \Delta TMV = G_e * \Delta TMV \qquad (6)$$

where g_e is the electroporation conductance of a single pore, N is the number of pores per unit membrane area, ΔTMV is the TMV relative to the resting voltage, and G_e is the total electroporation conductance. In this way, the conductance of a pore g_e is modeled as an instantaneous function of transmembrane potential:

$$g_e(V_m) = \frac{\pi * h * \sigma}{4} * \frac{e^{v_m} - 1}{e^{v_m} \frac{w_0 * e^{(w_0 - n*v_m)} - n * v_m}{w_0 - n * v_m} - \frac{w_0 * e^{(w_0 + n*v_m)} + n * v_m}{w_0 + n * v_m}} \qquad (7)$$

Equation (7) arises from the integration of the Nernst-Planck equation describing the one-dimensional movement of ions across the membrane [33][34], where h is the thickness of the membrane, σ is the conductivity of the aqueous solution that fills the pore, w_0 is the energy barrier within pore, and n is the relative entrance length of the pore. $v_m$is the nondimensional transmembrane potential, $v_m \equiv V_m \frac{e}{k*T}$, where e is the charge on an electron, k is the Boltzmann constant, and T is the absolute temperature.

In this description, it is assumed that the electroporation conductance is produced by pores of identical size and shape, and it is calculated as the conductivity of a cylindrical channel that represents an energetic barrier for ions. This energy barrier must be overcome for there to be ion conduction through the pore and, once this energy barrier is overcome, g_e saturates at its maximum value.

The number of pores per unit area N is governed by a first order differential equation:

$$\frac{dN}{dt} = \alpha * e^{\beta * (V_m)^2} * \left(1 - \frac{N}{N_0} e^{-q*\beta*(V_m)^2}\right) \qquad (8)$$

where N_0 is the number of pores per unit membrane area when $\Delta TMV = 0\ mV$, and α, β, and q are constants. Note that the electroporation parameters (α, β, N_0 and w_0) should be optimized for a given kind of membrane. The present study considers the parameters used in [21], which were adjusted from human erythrocyte and L-cell membranes [35], until the total root mean square error between the model and the experiment of Zhou et al., 1996 [36] was minimized. Therefore, the electroporation parameters used to solve equations (7) and (8) are reported in Table 4.

Table 4. Electroporation parameters.

Symbol	Value	Definition
h	$4 * 10^{-9}\ m$	Membrane thickness [28]
T	$310\ K$	Temperature
σ	1.3 S / m	Conductivity of aqueous solution in pores

n	0.15	Relative entrance length of pores
q	2.46	Electroporation constant
α	$2 * 10^9\ m^{-2}s^{-1}$	Electroporation parameter
β	$62.5\ V^{-2}$	Electroporation parameter
N_0	$1.5 * 10^9\ m^{-2}$	Pore density when ΔTMV = 0 mV
w_0	$5.25\ kT$	Energy barrier within pore
k	$1.38 * 10^{-23}\ m^2\ kg\ s^{-2}K^{-1}$	Boltzmann constant
e	$1.60 * 10^{-19}$ C	Electron charge

In this way, through this approach, the dynamics of the electroporation variables (ΔTMV, g_e, N, G_e, and I_e) can be evaluated, and their effect on nerve function under different conditions.

First, the different variables are evaluated in a single node, applying different voltage intensities between the electrodes (electroporation scenario), to evaluate their dynamics for different degrees of electroporation. Then, these dynamics are compared along the nerve fiber considering different degrees of electroporation in the general scenario. Finally, a conduction block protocol is carried out to evaluate how these variables can influence the nerve conduction. This protocol consists of a first stimulation of the medial nodes of the nerve fiber with different electroporation paradigms (electroporation scenario), and after 20 ms, a delivery of a subsequent distal stimulation (stimulation scenario) with a 0.5 V monophasic pulse with a duration of 100 μs. In this way, through this protocol, it is possible to evaluate the ability of the nerve to transmit an electrical signal after being affected by different degrees of electroporation.

c) KHFAC modeling

Furthermore, the KHFAC electrical waves are evaluated, to assess whether the blocking observed in experiments with these waveforms are a consequence of the electroporation effect on the membrane. The protocol to study the effects of these waveforms is as follows: an analogous blocking waveform to the one presented in [16] (3 kHz sinusoidal wave with amplitude of 10 V_{pp}) is delivered to the medial nodes of the nerve fiber (electroporation scenario) for 30 ms. Afterwards, the dynamics and magnitude of the electroporation variables are evaluated to assess if their values are compatible with blocking effects.

2.4. Conduction velocity ($\boldsymbol{CV}$) determination

As explained previously, in a nerve fiber, a local point of depolarization causes ionic movement between adjacent points on the axon, thus propagating the region of depolarization (see Figure 4). The CV depends on the rate at which electrical charge is transferred from the locus of excitation to the region of membrane ahead of the AP, and the charge-transfer rate, in turn, depends on the membrane capacity and the longitudinal resistance of the axon [37]. However, they are considered the same under all conditions (see Table 3).

In this way, the CV determinations were made by dividing the conduction distance by the conduction latency between two nodes of the nerve fiber:

$$Conduction\ velocity\ (CV) = \frac{Conduction\ distance}{Conduction\ latency} \qquad (9)$$

The conduction latency is set as the time elapsed between the triggering of the action potentials in two different nodes of the nerve fiber. Note that it is considered that an action potential had been triggered in a node when the sodium current across the membrane showed a large and fast increase at this node. In this way, it is considered that one node is triggering an action potential when its gating parameter for the sodium current m > 0.8 (see section SI-1. Equations describing the ionic currents) [2].

3. RESULTS

3.1. Constant electroporation conductance

a) Blocking analysis

Figure 10 shows the CV calculated between nodes 10 and 60, considering different constant values of G_e only in the central nodes of the fiber (nodes 38-48), after stimulating the right nodes of the nerve fiber (stimulation scenario) with a 0.5 V monophasic pulse with a duration of 100 µs. As shown, CV decreased as G_e increased, and for G_e = 2379 S / m^2 (G_e threshold), the propagation of the action potential was completely blocked (CV = 0 m / s).

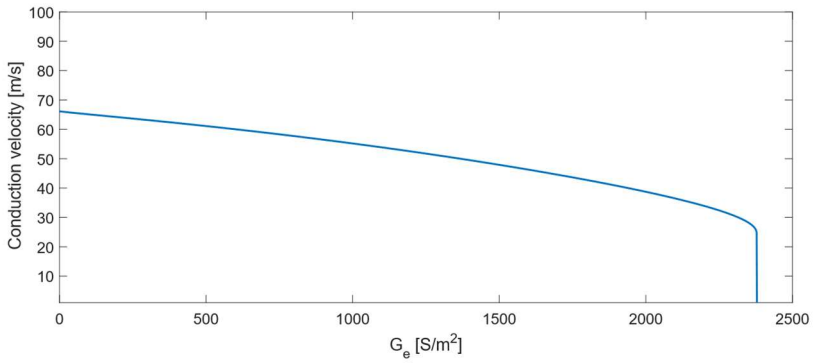

Figure 10. Conduction velocity vs. electroporation conductance stimulating the right nodes with a 0.5 V monophasic pulse with a duration of 100 µs. G_e considered in nodes 38-48

This conduction block is observable in Figure 11, in which the ΔTMV along the time at all nodes is represented in two conditions: without considering G_e (control, see Figure 11 (A)), and considering G_e threshold (see Figure 11 (B)). In the second case, the conduction block occurred in the central nodes were G_e was added (red arrow).

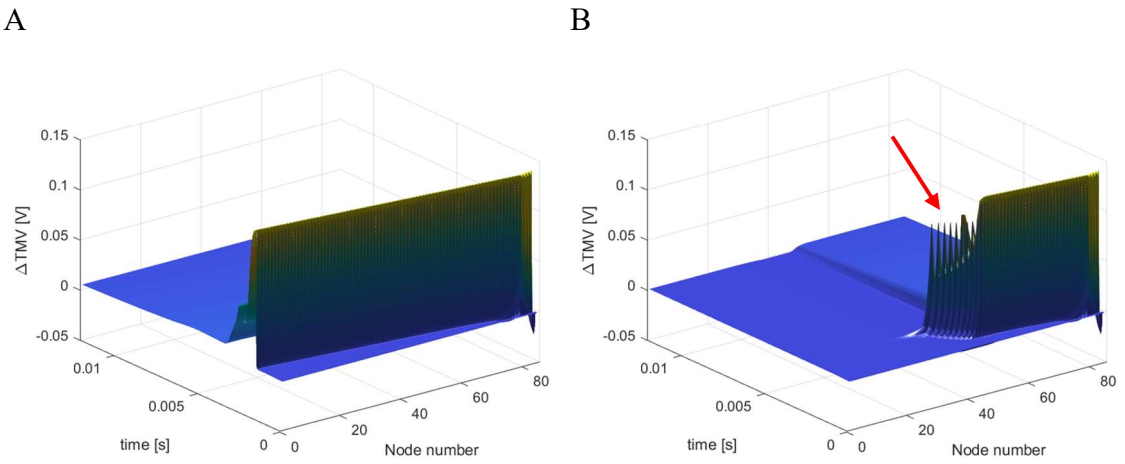

*Figure 11. ΔTMV along the nodes in each time step stimulating the right nodes with a 0.5 V monophasic pulse with a duration of 100 µs. G_e considered in nodes 38-48. **A**: without considering electroporation conductance (G_e = 0 S / m^2). **B:** considering G_e threshold (G_e = 2379 S / m^2). The red arrow indicates the block of the action potential propagation.*

Therefore, with this evaluation, it was demonstrated that the electroporation phenomenon decreases the conduction velocity in nerve fibers and, for values of G_e suficiently high (> 2379 S / m^2), the propagation of the AP along them is completely blocked.

b) Excitability analysis

In this analysis, the excitability of a nerve fiber was assessed considering different constant values of G_e in all nodes, stimulating the nerve fiber through the general scenario with a 100 µs monophasic pulse. Figure 12 shows that the minimum voltage difference between the electrodes at which the nerve fiber triggers an action potential increased linearly with G_e. Thus, this reflected that the electroporation phenomenon influences the nerve's excitability by increasing its voltage threshold.

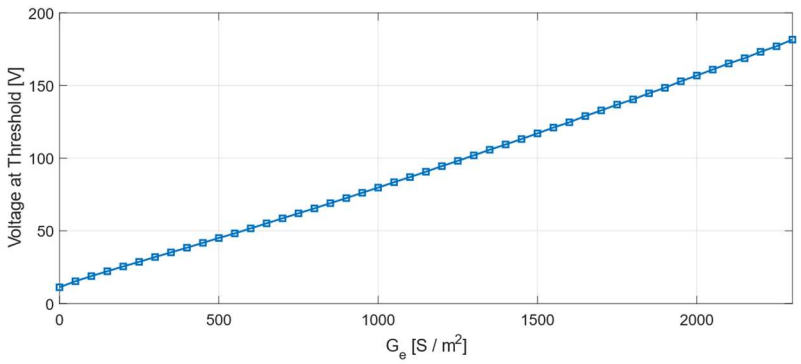

Figure 12. G_e vs. stimulation threshold. Stimulating the nerve fiber through the general scenario with a monophasic pulse with a duration of 100 µs

Besides, a blocking analysis was carried out in this context (G_e included in all nodes), and a situation like when stimulating the right nodes was obtained. Figure 13 shows the CV

calculated between nodes 4 and 20, considering different constant values of G_e in all nodes. In this way, CV decreased as G_e increased. Finally, for G_e = 1275 S / m^2 (G_e threshold), the propagation of the action potential was completely blocked (CV = 0 m / s).

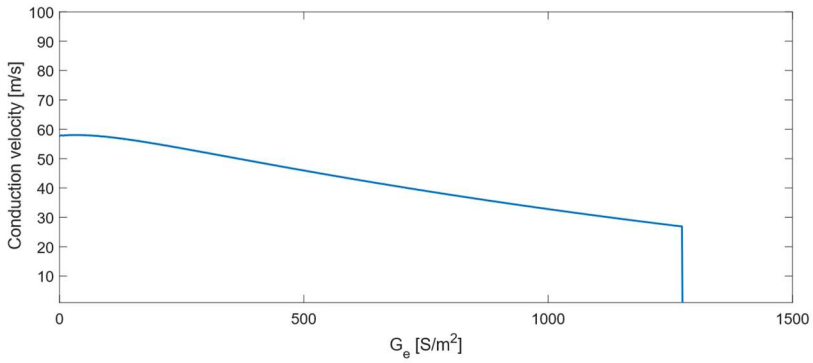

Figure 13. Conduction velocity vs. electroporation conductance. Stimulating the nerve fiber through the general scenario with a 100 V monophasic pulse with a duration of 100 µs. G_e considered in all nodes.

In Figure 14, the action potential propagation along the nerve fiber is compared between the conditions in which G_e is not considered (control, see Figure 14 (A)), and when G_e threshold is considered (see Figure 14 (B)). In the latter case, despite being changes in the TMV of the nodes close to the electrodes, no APs were generated in any node of the nerve fiber. Therefore, the nerve fiber lost its excitability in this condition.

A B

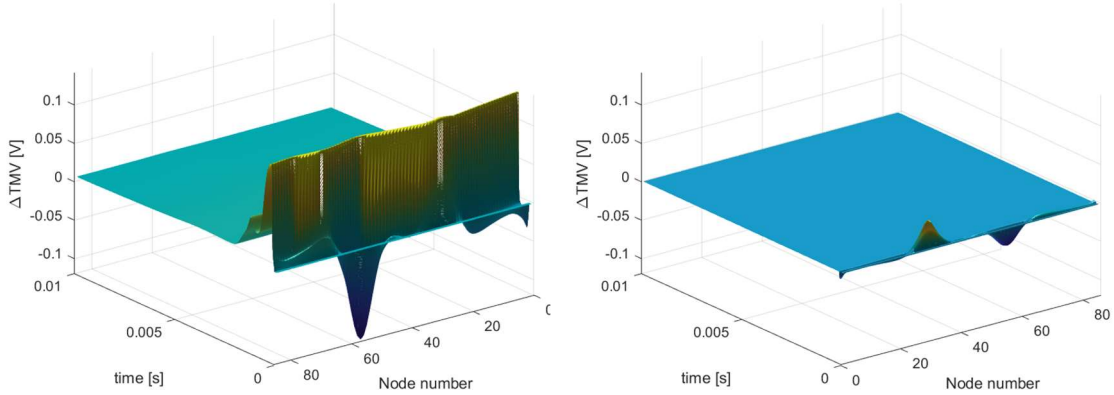

*Figure 14 ΔTMV along the nodes in each time step. Stimulating the nerve fiber through a 100 V monophasic pulse with a duration of 100 µs. G_e in all nodes. **A**: without considering electroporation conductance (G_e = 0 S / m^2). **B**: considering G_e threshold (G_e = 1275 S / m^2).*

3.2. Dynamic electroporation conductance

a) Analysis of electroporation variables

First, g_e dependency on the nondimensional transmembrane potential (v_m) was assessed to study its non-linearity. Figure 15 shows that when v_m tends to zero, g_e tends to zero.

However, for higher values of v_m, g_e saturates around $3.8 * 10^{-9}$ S. The model assumes that the conductivity of the membrane is produced by pores of identical size and shape, and it is calculated as the conductivity of a cylindrical channel that represents an energetic barrier for ions. Thus, this saturation indicated that for high v_m values, the energy barrier is overcome.

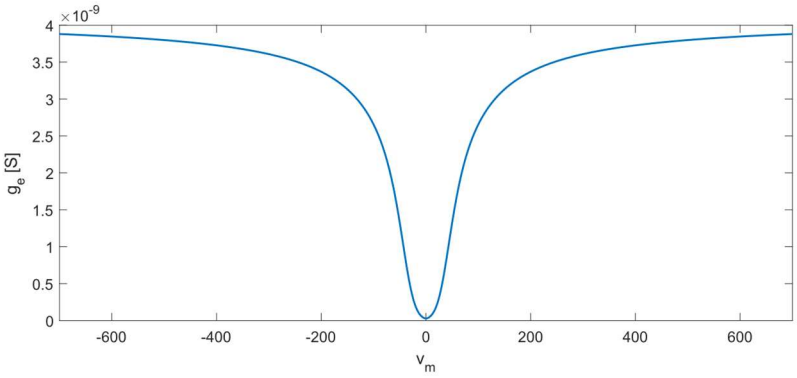

Figure 15. g_e dependency on v_m

To validate the implementation of dynamic electroporation conductance in the cable model, it was first assessed the ΔTMV dynamics after applying different strength voltages between the electrodes in the medial nodes (electroporation scenario). For this analysis, the cable model was reduced to a model only including the electroporation (i.e. it was assumed that the membrane was not excitable, and ionic currents were eliminated). Therefore, only I_e was considered in the cable model (no ionic currents and leakage current), and the ΔTMV was evaluated at the node closest to the cathode (41). Figure 16 shows the results for the evolution of the ΔTMV for different applied voltages. Comparing the results presented by W. Krassowska 1995 [20], the ΔTMV follows similar dynamics during the pulse application: for low external voltages (5 and 10 V), the ΔTMV follows the expected behavior of a charging membrane, and its values increase with the strength of the applied voltage, while for higher voltages (15 and 20 V), the behavior changes, and the expected increase of the transmembrane potential was inhibited by the electroporation effect. Therefore, these higher voltages electroporated the membrane, decreasing the normal membrane resistance (short circuited), and consequently, producing a self-regulation of the TMV.

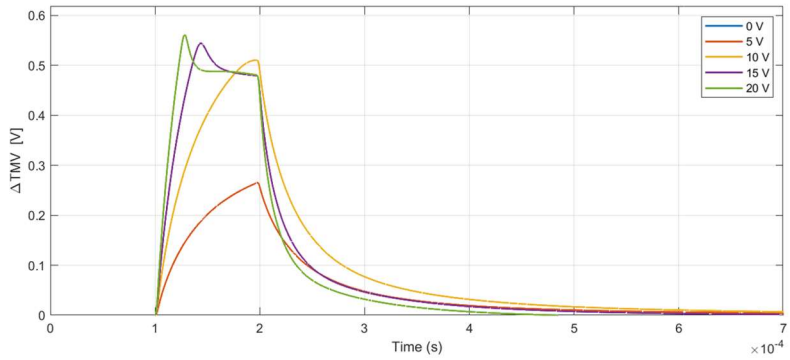

Figure 16. Time course of the ΔTMV at node 41 of the nerve fiber after stimulating the medial nodes with different strength voltages between the electrodes.

To understand the basis of this effect, Figure 17 shows the time course of the elecroporation variables (g_e, N, G_e, and I_e), which are directly involved in the electroporation. g_e incresaes with the applied external voltage strenght. For higher voltages (10, 15, and 20 V), the energy barrier was overcome, and g_e became almost saturated at its maximum value ($= 3.8 * 10^{-9}$ S). N also increased with the applied strength of the external voltage, and its effects were much more significant at higher voltages. For 5 V, N was close to N_0 (pore density for ΔTMV = 0 V, see Table 4). Then, since G_e is the product of g_e and N, and there was no significant difference among g_e values of the different applied voltage strengths, G_e was the result of scaling g_e with its respective N. Finally, since I_e is the result of multiplying G_e by the ΔTMV, it was only noticeable during the application of the pulse (non-zero values of ΔTMV). Interestingly, since N decreased slowly (pore resealing process is not noticeable in the represented timescale), this electroporation effect will still be present in subsequent nerve fiber stimulations.

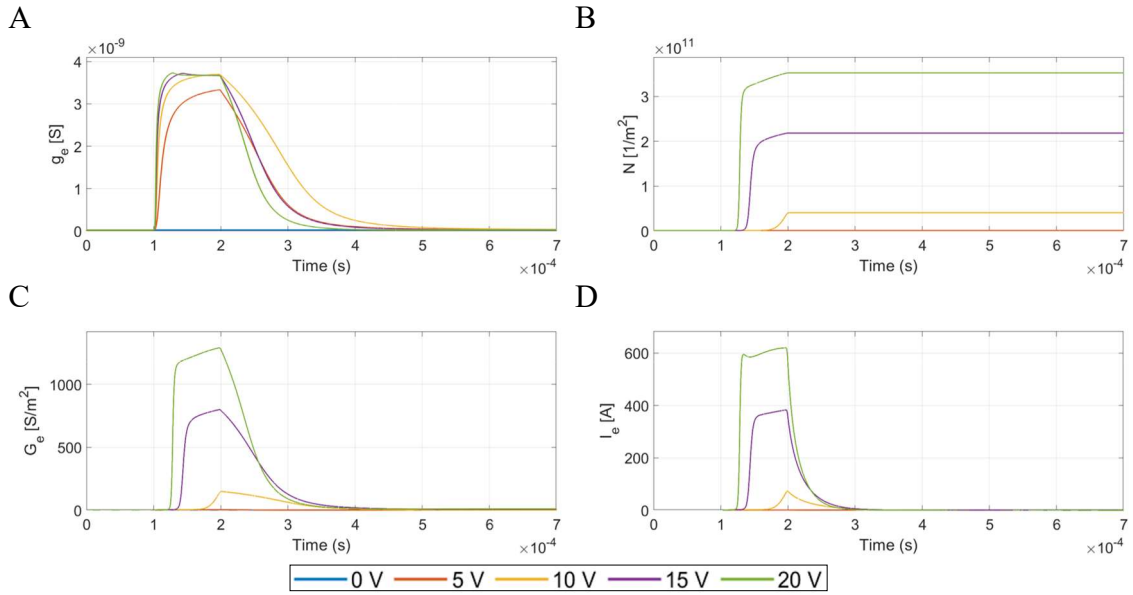

Figure 17. Time course of g_e (**A**)*, N* (**B**)*, G_e* (**C**)*, and I_e* (**D**) *at node 41 of the nerve fiber stimulating the medial nodes with different strength voltages between the electrodes.*

To understand the effect of electroporation, it is important to evaluate the dynamics of these variables considering different degrees of electroporation. In this way, two situations were assessed after stimulating the nerve fiber through the general scenario. On the one hand, Figure 18 shows the temporal evolution of ΔTMV, g_e, N_e, G_e, and I_e in all nodes, after stimulating the nerve fiber with a 100 V monophasic pulse with a duration of 100 µs between the electrodes. One the other hand, Figure 19 shows the same variables after delivering 1000 V monophasic pulse with a duration of 100 µs. Note that in this analysis, it was still considered that the only current flowing through the membrane is the electroporation current (ionic and leakage currents not considered), in order to assess the electroporation variables without the influence of the ionic currents.

First, ΔTMV presented higher values (in absolute value) in the 1000 V condition, and the higher ones were at the nodes closest to the electrodes in both conditions. Furthermore, in the 1000 V condition, g_e had higher values throughout the fiber, while when stimulating with 100 V, only high values of g_e (but under saturation levels) were obtained in the nodes close the electrodes. Then, in the 100 V condition, N increased only in the

nodes near the electrodes, but the increase from N_0 is very small, suggesting that the level of electroporation, if any, was very low. However, in the 1000 V condition, N increased two orders of magnitude from N_0 at the nodes near the electrodes. Consequently, G_e presented the higher values in these nodes, and its magnitude was much higher when stimulating with 1000 V. However, these values are high only during the pulse application. Finally, I_e increased in absolute value in the nodes near the electrodes during the application of the pulse, and it presented a similar dynamic in both conditions (positive values in nodes near the cathode, and negative values in nodes near the anode). However, the I_e in the 1000 V condition also presented higher values by three orders of magnitude.

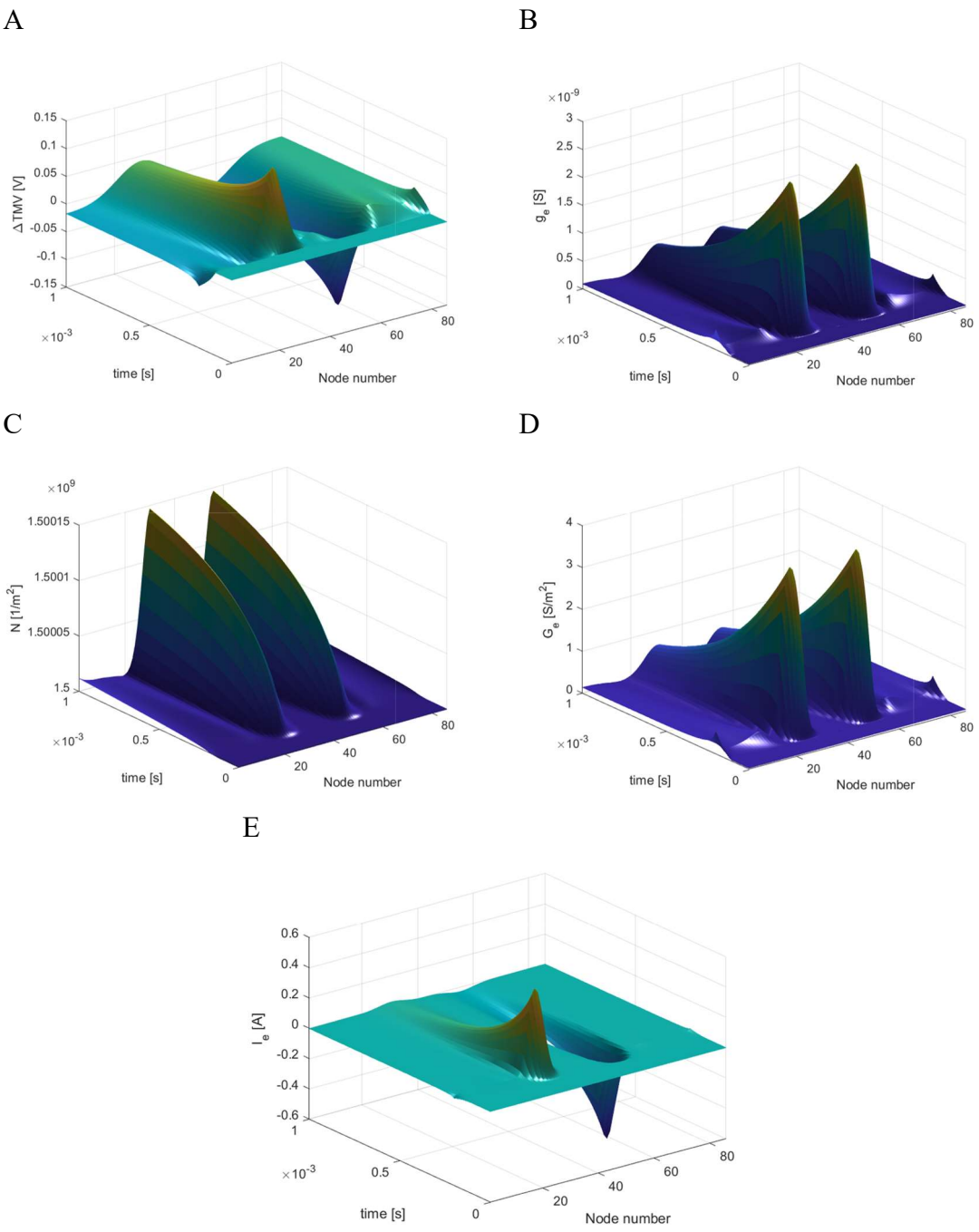

*Figure 18. Time course of ΔTMV (**A**), g_e (**B**), N (**C**), G_e (**D**), and I_e (**E**) at all nodes after stimulating the nerve fiber with a 100 V monophasic pulse with a duration of 100 μs in the general scenario.*

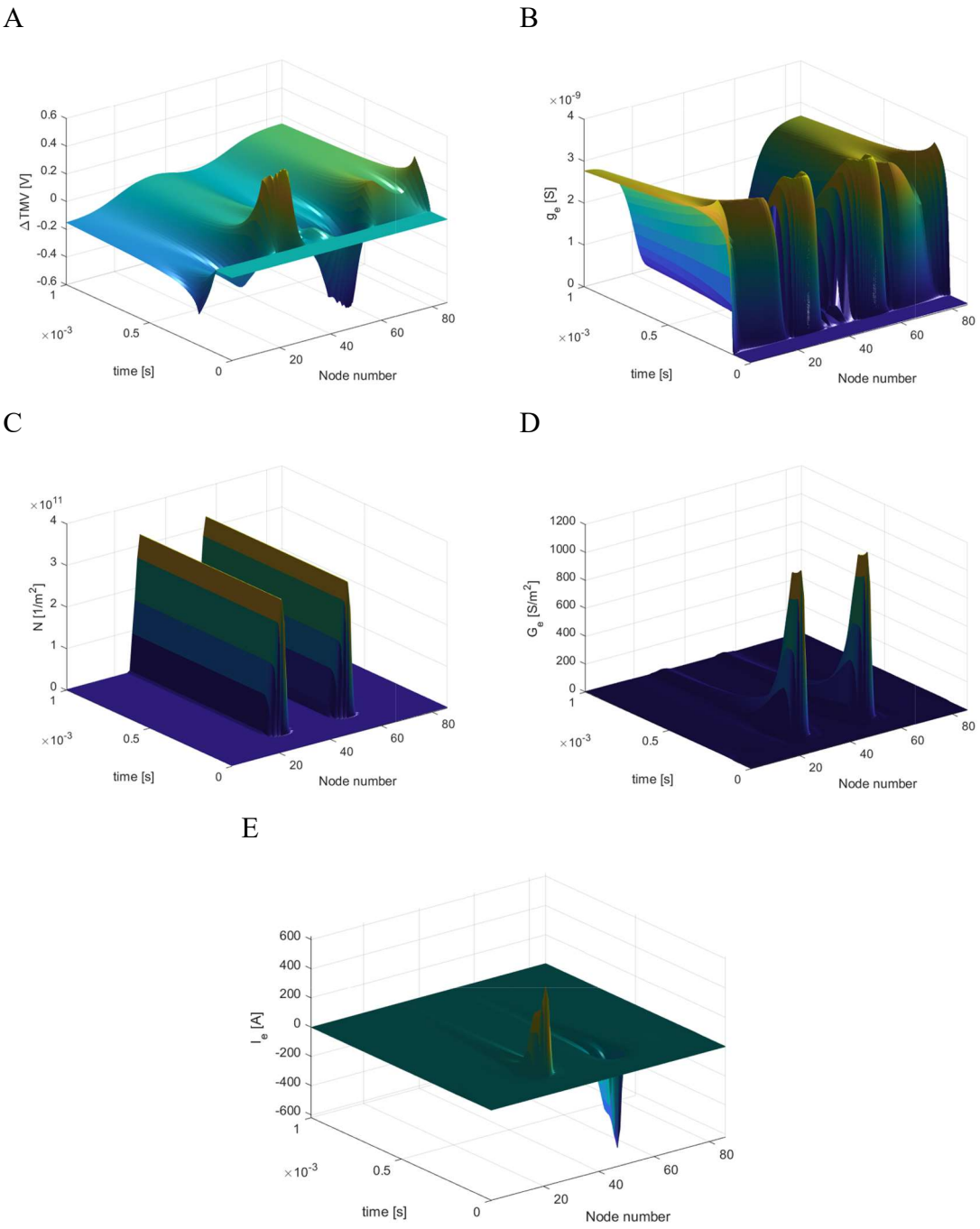

*Figure 19. Time course of ΔTMV (**A**), g_e (**B**), N (**C**), G_e (**D**), and I_e (**E**) at all nodes after stimulating the nerve fiber with a 1000 V monophasic pulse with a duration of 100 µs in the general scenario.*

In this way, by delivering 1000 V the nerve fiber membrane was clearly electroporated: g_e had maximum saturation values values in the whole fiber, and N increased a lot from N_0, producing a significant increase on G_e and I_e.

b) Conduction block protocol

To evaluate how the electroporation variables influence on the nerve fiber function, a conduction block protocol was performed. Figure 20 compares the dynamics of g_e, N, G_e, I_e, and ΔTMV at node 41 during 1 ms, after exposing the medial nodes of the nerve fiber (electroporation scenario) applying 15 or 350 V monophasic pulses with a duration of 100 µs between the electrodes. Note that in this first part of the protocol, it was assumed that the membrane was not excitable (only electroporation current), in order to assess the electroporation variables without producing APs. We acknowledge that this situation is not realistic, but it was considered in this analysis for simplification.

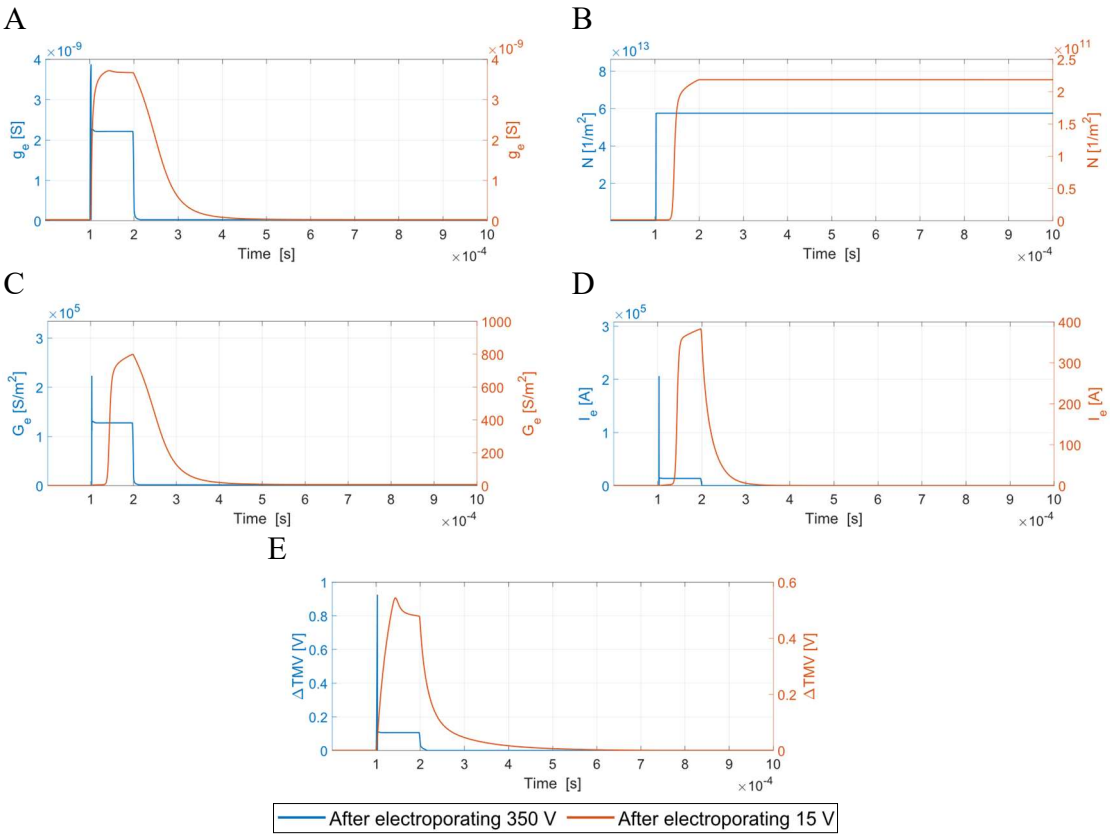

Figure 20. 1 ms time course of g_e (**A**), *N* (**B**), *G_e* (**C**), *I_e* (**D**), and ΔTMV (**E**) *at node 41 after electroporating the middle nodes with a 15 V monophasic pulse with a duration of 100 µs vs. after electroporating with a 350 V monophasic pulse with a duration of 100 µs.*

In both conditions (15 and 350 V), g_e peak was close to $3.8 * 10^{-9}$ S. Therefore, the conductivity in a single pore was saturated at its maximum value in both conditions. However, the pore formation was more significant when 350 V was applied, since N was two orders of magnitude higher than when applying 15 V. Nervetheless, despite having pore resealing, it was not significant during the simulation. Finally, G_e and I_e peaks were three orders of magnitude higher when electroporating with 350 V.

As mentioned above, electroporation produces self-regulation in ΔTMV. In Figure 20 (E) it is shown how this short circuit was very pronunced in the 350 V condition, and consequently, it influenced directly on the dynamics of g_e, G_e, and I_e. Nevertheless,

despite this self-regulation, the peak magnitude was always higher in all the electroporation variables in the 350 V condition.

After 20 ms [3] of electroporation of nerve fibers with different electroporation strenghts (15 or 350 V), the distal nerve nodes (stimulation scenario) were stimulated, with a 100 µs monophasic pulse with 0.5 V between the electrodes, in order to assess the fiver's ability to propagate APs after being electroporated. Now, since the APs propagation was being evaluated, it was assumed that the membrane was excitable (ionic and leakage currents considered), and electroporable (I_e was also considered).

Figure 21 (A) shows the time course of ΔTMV at all nodes after the distal stimulation in the nerve fiber previously electroporated with 15 V, and Figure 21 (B) shows the time course of ΔTMV at all nodes after the distal stimulation in a non-electroporated nerve fiber (control). The CV in the electroporated fiber only decreased 0,21 m / s with respect to the control. Therefore, the maginude of the electroporation variables regarding to this condition showed in Figure 20 did not have a significant impact on the nerve's ability to propagate an AP.

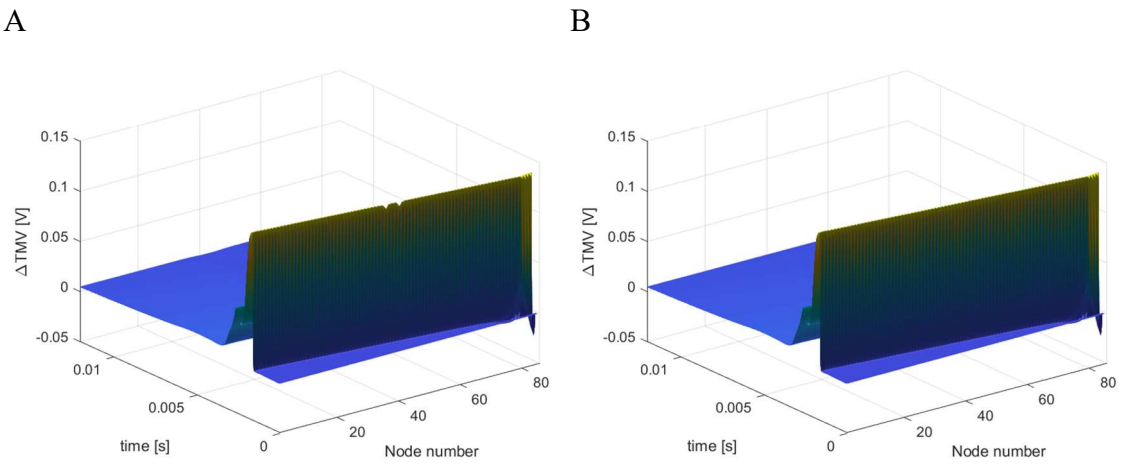

*Figure 21. Time course of ΔTMV at all nodes. (**A**) Stimulating the right nodes with a 0.5 V monophasic pulse with a duration of 100 µs after a previous electroporation of the nerve with a 15 V monophasic pulse with a duration of 100 µs (CV = 65.46 m / s). (**B**) Stimulating the right nodes with a 0.5 V monophasic pulse with a duration of 100 µs, without a previous electroporation of the nerve (CV = 65.67 m / s).*

On the other hand, the same analysis was carried out in the electroporated nerve with 350 V. In this case, Figure 22 (A) shows how the AP propagation in the previously electroporated nerve is completely blocked in the nodes near the electrodes (red arrow). Thus, the magnitudes of the electroporation variables of this condition, exposed in Figure 20, have a blocking effect on the nerve. As shown in Figure 20, most of the variables recover back to their initial levels shortly after pulse application, the only variable that remains considerably high after the pulse delivery is N (number of pores). Thus, this variable is responsible for the blocking effect shown in Figure 22.

[3] Electroporation pulses were simulated for 20 ms. However, the relevant dynamics occurs during and just after the application of the pulses. Therefore, Figure 20 only shows the dynamics in 1 ms.

A B

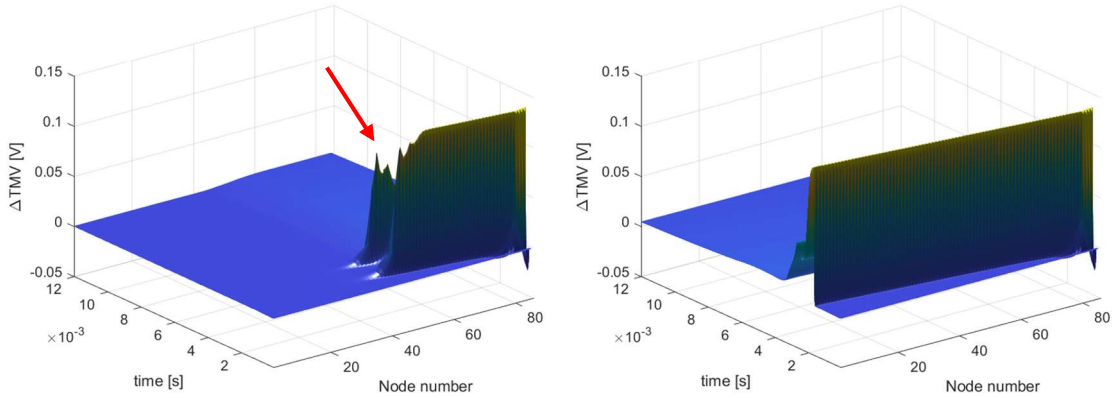

*Figure 22. Time course of ΔTMV at all nodes. (**A**) Stimulating the right nodes with a 0.5 V monophasic pulse with a duration of 100 µs after a previous electroporation of the nerve with a 350 V monophasic pulse with a duration of 100 µs (CV = 0 m / s). (**B**) Stimulating the right nodes with a 0.5 V monophasic pulse with a duration of 100 µs, without a previous electroporation of the nerve (CV = 65.67 m / s).*

c) KHFAC modeling

Figure 23 shows the dynamics of the electroporation variables at node 41 during the application of a 3 kHz sinusoidal wave with an amplitude of 10 V_{pp} in the medial nodes (electroporation scenario) for 30 ms, in order to assess whether the KHFAC block presented in [16] can be explained by the electroporation phenomenon. Figure 24 zooms in the simulation from 0 to 4 ms to assess the dynamics in detail. Note that in this analysis, it was assumed that the only current through the membrane was the electroporation current (ionic and leakage currents not included in the model), to evaluate the electroporation variables without the influence of the ionic currents.

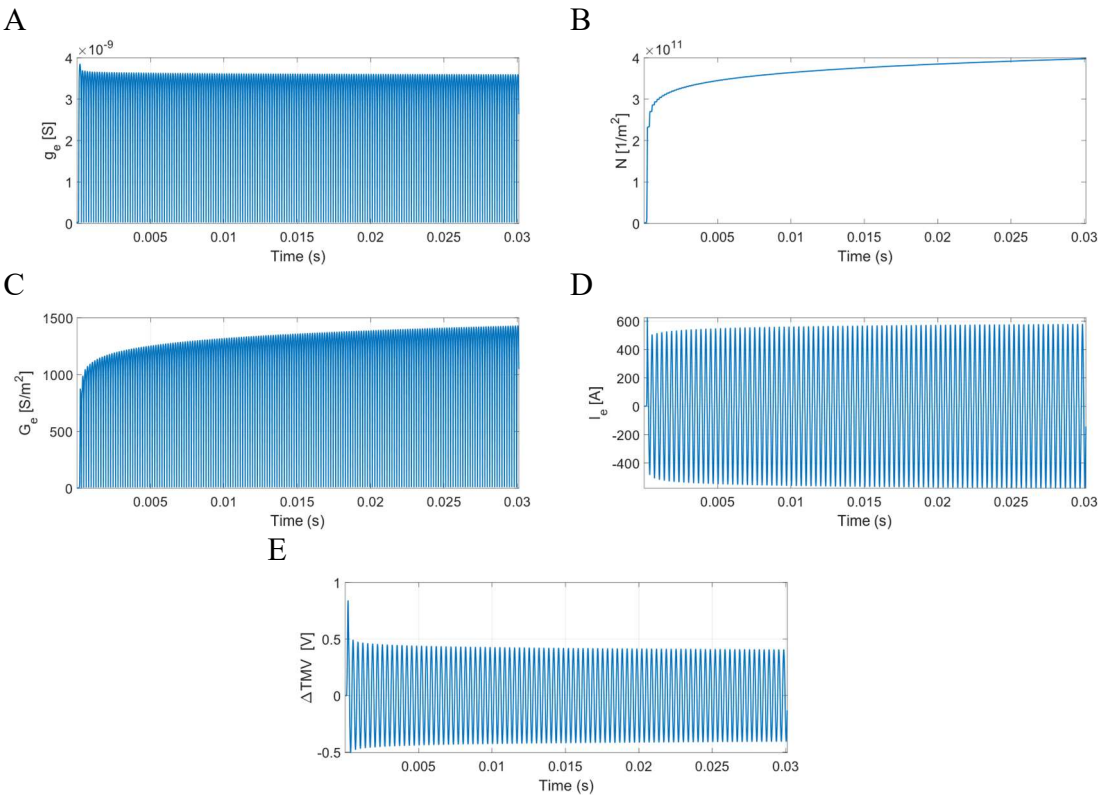

Figure 23. Time course of g_e (**A**)*, N* (**B**)*, G_e* (**C**)*, I_e* (**D**), and ΔTMV (**E**) *at node 41 when electroporating with a KHFAC sine wave of 3 kHz with an amplitude of 10 V_{pp}*

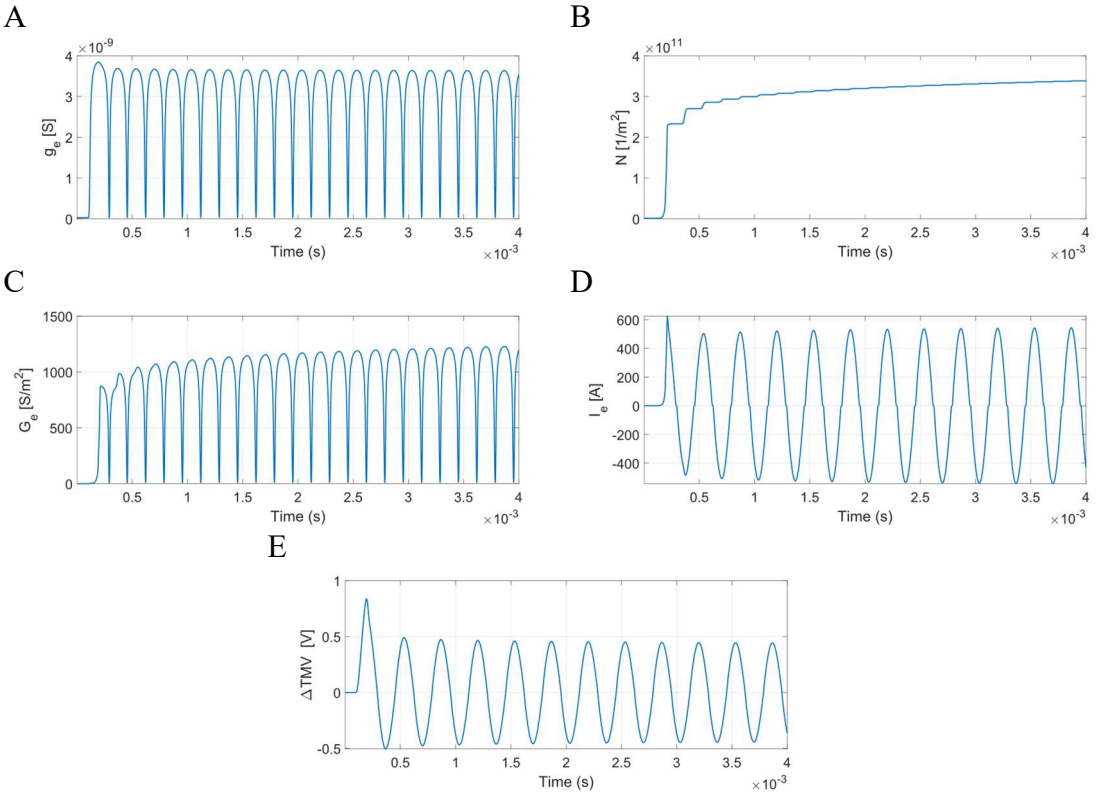

Figure 24. Zoom in the time course of g_e (**A**)*, N* (**B**)*, G_e* (**C**)*, I_e* (**D**), and ΔTMV (**E**) *at node 41 when electroporating with a KHFAC sine wave of 3 kHz with an amplitude of 10 V_{pp}.*

The ΔTMV presented an absolute maximum when the stimulus was applied, and then it presented an oscillating behavior with their amplitudes decreasing a little in time. This effect may be caused by the saturation (short circuit) of the transmembrane potential during electroporation. g_e also exhibited an oscillating behavior, having maximum values in the extremes of the applied sine wave. On the other hand, N exhibited a significant increase when the stimulus was applied, and it still grew during the entire application of the stimulus. In this way, G_e and I_e presented the oscillating dynamics of the other electroporation variables, but their amplitudes increase with time due to the incremental magnitude of N.

The blocking capacity of the KHFAC wave can be determined by evaluating the magnitude of the electroporation variable G_e. Remember that during the blocking analysis performed previously with constant electroporation conductance (see section a) Blocking analysis), the $G_e$threshold to block a distal stimulation was 2379 S / m^2. In this way, during the KHFAC modeling, the maximum value of G_e was around 1400 S / m^2 (see Figure 23 (C)), which would not present a blocking effect, but it is quite high. However, due to the high growth rate of G_e, it could reach blocking values after few seconds (note that in Kilgore et. al., 2004 [16] the blocking stimulation was carried out for 40 s). In this modeling, such long simulations times would not be possible due to the heavy computational load.

Furthermore, in the KHFAC blockade study [16], the sine wave application was accompanied by proximal stimulations of 10 μA monophasic pulses lasting 200 μs at 0.2 Hz during the KHFAC delivery, and such stimulations might contribute significantly on electroporating nerves. However, the present model cannot simulate the nerve fiber dynamics when multiple and consecutive electric fields are delivered.

In addition, the magnitude of G_e was evaluated increasing the amplitude of the KHFAC block to 15 V_{pp}, to assess whether it would be possible to obtain blocking effects if the amplitude of the KHFAC is increased a little. Figure 25 shows the dynamics of G_e at node 41 during the application of a 3 kHz sinusoidal wave with amplitude of 15 V_{pp} in the medial nodes (electroporation scenario). In this context, G_e reaches values higher than 2379 S / m^2 (G_e threshold obtained to block a distal stimulation) and therefore, it would have a blocking effect on the propagation of action potentials.

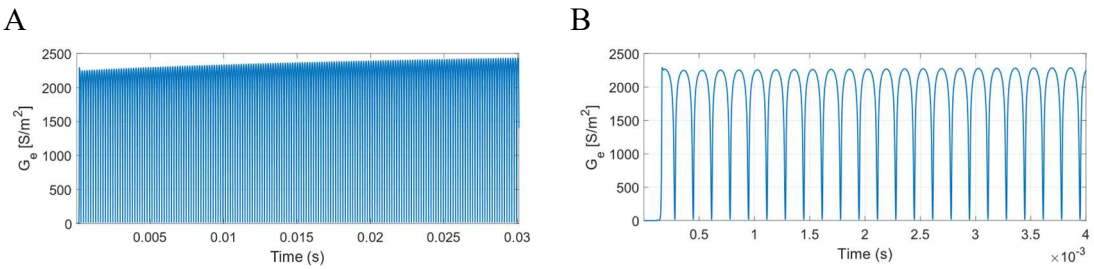

*Figure 25. **A**: time course of G_e at node 41 when electroporating with a KHFAC sine wave of 3 kHz with an amplitude of 15 V_{pp}. **B**: zoom in the time course of G_e at node 41 when electroporating with a KHFAC sine wave of 3 kHz with an amplitude of 15 V_{pp}*

In this way, the KHFAC observed in [16] could be explained as consequence of the effect of electroporation on the cell membrane. Further modelization should be performed to understand this phenomenon in detail.

4. DISCUSSION

Regarding to the approach of the constant G_e modeling, the results in the blocking analysis indicated that the electroporation phenomenon alters the ability of nerve fibers to propagate APs, being able to reduce its conduction velocity and, for high electroporation strengths, completely arrest the propagation of the AP along it. On the other hand, in the excitation analysis, the results showed that the electroporation phenomenon directly influences the excitability of the nerve, reducing its capability to trigger action potentials.

In this way, the results obtained through the blocking analysis, suggested that the reduction of the conduction velocity after the external application of electric fields in Abramov et. al., 1996 [13], can be explained by the primary effect of electroporation on the membrane. Furthermore, the results obtained by the excitability analysis, suggest that the reduction in muscle force after the external application of electric fields observed in H- Gissel et. al., 2002 [14] and T. Clausen et. al., 2005 [15], can be also explained by the electroporation phenomenon.

In addition, the implemented dynamic model of the electroporation conductance was validated, and the temporal dynamics of the electroporation variables were evaluated for different degrees of electroporation and conduction block. For low pulse strengths (under the electroporation threshold), the ability of the nerve fiber to propagate APs was not affected, while for high enough pulse strengths (over the electroporation threshold), the nerve fiber lost this ability.

Note that due to computational weight restrictions, the pore resealing dynamics could not be fully studied to understand the dynamics of N after the pulses. However, N increased greatly in magnitude from N_0 when the external stimulus amplitude was enough to electroporate the membrane, and resealing appeared to be a slow process. Therefore, by extrapolating the decrease in N during resealing, it can be concluded that this first electroporation would impact subsequent stimulations produced seconds later.

Subsequently, using the implemented dynamic model, KHFAC blockade was evaluated to reason whether the experimental findings presented in Kilgore et. al., 2004 [16] and Bhadra et. al., 2005 [17] can be explained by the electroporation phenomenon. The results suggested that in an analogous situation to [16], G_e would not reach blocking values in the first 30 ms of KHFAC delivery. However, due to the observed growth rate of the variable over time, it could reach blocking values after few seconds (note that in [16] the blocking stimulation was carried out during 40 s). Furthermore, note that the modeled KHFAC block [16], was accompanied by proximal stimulations of 10 μA monophasic pulses lasting 200 μs at 0.2 Hz parallelly to the KHFAC delivery, and such stimulations might also contribute significantly on electroporating nerves. This last effect should be studied separately. Although this preliminary study suggests that the KHFAC block could be explained at least in part as a consequence of the effect of electroporation on the cell membrane, a more detailed analysis considering more variables (e.g. ionic currents and proximal stimulations) would be necessary to have a more consolidated conclusion.

Finally, is worth mentioning that as a further work, the model of the dynamic electroporation should be implemented simultaneously with the complete nerve fiber

model (with the ionic and leakage currents) during electroporation pulses. Also, more complete nerve fiber models including the resting period as the one presented in C.C. McIntyre et. al., 2002 [26] could be used in the future. In this way, it would be possible to carry out a complete *in-silico* analysis of the KHFAC blockade.

This kind of modeling could add value in clinical practice. It is known that treatment planning is essential for successful electroporation, and the current treatment planning models focus primarily on the position of the electrodes, and the calculation of the electric field distribution to cover the target tissue with electric fields and preserve the non-target tissue [1]. However, such models do not consider the possible muscle contractions and acute pain that appear during these treatments. If a model could predict if large nerve fibers could be electroporated (leading to a loss of their excitability and/or loss of their capability to propagate APs), this could be used to develop new pulse delivery protocols, where a first pulse sequence would be designed to deactivate nerve fibers, and subsequently electroporation pulses could be applied without the collateral contractions and associated pain. Of course, the electroporation parameters must be previously optimized to different sorts of nerves.

5. CONCLUSION

After numerically modeling the effect of electroporation on nerve fiber function, the reduction of the conduction velocity in nerve fibers, and the reduction of muscle force observed in some experiments after the application of pulsed electric fields of large magnitude, have been explained to be the consequence of electroporation on the cell membrane. Besides, it has been demonstrated for the first time that the conduction block produced by low voltage and high duration kilohertz frequency alternating currents (KHFAC) observed in some studies could be also related to electroporation of nerve fibers. In this way, it can be concluded that the proposed hypotheses are plausible; electroporation can alter the functionality of nerve fibers by reducing their ability to propagate APs, blocking the AP propagation, and reducing their excitability.

BIBLIOGRAPHY

[1]. M. L. Yarmush, A. Golberg, G. Sersa, T. Kotnik, and D. Miklavcic, “Electroporation-Based Technologies for Medicine: Principles, Applications, and Challenges," Annual Review of Biomedical Engineering, vol. 16, no. 1, pp. 295-320, jul 2014.

[2]. Mercadal Cavaller, Borja. Electroporation and peripheral nerve stimulation. 2019. https://www.tdx.cat/handle/10803/667854#page=1

[3]. M. Cemazar, “Effects of electroporation of mammalian cells on cytoskeleton and intercellular connections,” in. Jan. 2016. doi: 10.1007/978-3-319-26779-1_18-1.

[4]. L. C. Heller and R. Heller, \Electroporation Gene Therapy Preclinical and Clinical Trials for Melanoma," Current Gene Therapy, vol. 10, no. 4, pp. 312-317, aug 2010.

[5]. L. Low, A. Mander, K. McCann, D. Dearnaley, T. Tjelle, I. Mathiesen, F. Stevenson, and C. H. Ottensmeier, DNA Vaccination with Electroporation Induces Increased Antibody Responses in Patients with Prostate Cancer," Human Gene Therapy, vol. 20, no. 11, pp. 1269-1278, nov 2009.

[6]. Lee EW, Chen C, Prieto VE, Dry SM, Loh CT, Kee ST. 2010. Advanced hepatic ablation technique for creating complete cell death: irreversible electroporation. Radiology 255:426–33

[7]. B. Mercadal, C. Arena, R. Davalos, and A. Ivorra, “Avoiding nerve stimulation in irreversible electroporation: A numerical modeling study,” Physics in Medicine and Biology, vol. 62, pp. 8060–8079, 2017. doi: https://doi.org/10.1088/1361-6560/aa8c53

[8]. B. Rubinsky, “Irreversible electroporation in medicine,” Technology in Cancer Research & Treatment, vol. 6, no. 4, pp. 255–259, 2007, PMID: 17668932. doi: 10.1177/153303460700600401.

[9]. V. Y. Reddy, P. Neuzil, J. S. Koruth, J. Petru, M. Funosako, H. Cochet, L. Sediva, M. Chovanec, S. R. Dukkipati, and P. Jais, “Pulsed field ablation for pulmonary vein isolation in atrial fibrillation,” Journal of the American College of Cardiology, vol. 74, no. 3, pp. 315–326, 2019. doi: 10.1016/j.jacc.2019.04.021.

[10]. C. Ball, K. Thomson, and H. Kavnoudias, “Irreversible electroporation: A new challenge in "out of operating theater" anesthesia,” Anesthesia and analgesia, vol. 110, pp. 1305–9, Feb. 2010. doi: 10.1213/ANE.0b013e3181d27b30.

[11]. A. C. Guyton and J. E. Hall, Textbook of Medical Physiology, 10th ed. Philadelphia: W.B. Saunders Company, 2000.

[12]. C. Heckman and R. M. Enoka, “Motor Unit,” in Comprehensive Physiology. Hoboken, NJ, USA: John Wiley & Sons, Inc., oct 2012, col. 2, no. 4, pp. 2629-2682.

[13]. Abramov GS, Bier M, Capelli-Schellpfeffer M, Lee RC. Alteration in sensory nerve function following electrical shock. Burns. 1996 Dec;22(8):602-6. doi: 10.1016/s0305-4179(96)00055-1. PMID: 8982537

[14]. Gissel H, Clausen T. Ca2+ uptake and cellular integrity in rat EDL muscle exposed to electrostimulation, electroporation, or A23187. Am J Physiol Regul Integr Comp Physiol. 2003 Jul;285(1):R132-42. doi: 10.1152/ajpregu.00196.2002. Epub 2003 Mar 6. PMID: 12623773

[15]. Clausen T, Gissel H. Role of Na,K pumps in restoring contractility following loss of cell membrane integrity in rat skeletal muscle. Acta Physiol Scand. 2005 Mar;183(3):263-71. doi: 10.1111/j.1365-201X.2004.01394.x. PMID: 15743386

[16]. Kilgore KL, Bhadra N. Nerve conduction block utilising high-frequency alternating current. Med Biol Eng Comput. 2004 May;42(3):394-406. doi: 10.1007/BF02344716. PMID: 15191086.

[17]. Bhadra N, Kilgore KL. High-frequency electrical conduction block of mammalian peripheral motor nerve. Muscle Nerve. 2005 Dec;32(6):782-90. doi: 10.1002/mus.20428. PMID: 16124008.

[18]. Walsh AJ, Tolstykh GP, Martens S, Ibey BL, Beier HT. Action potential block in neurons by infrared light. Neurophotonics. 2016 Oct;3(4):040501. doi: 10.1117/1.NPh.3.4.040501. Epub 2016 Dec 1. PMID: 27990450; PMCID: PMC5140263.

[19]. Alex J. Walsh, Gleb P. Tolstykh, Stacey L. Martens, Bennett L. Ibey, and Hope T. Beier "Short infrared laser pulses block action potentials in neurons", Proc. SPIE 10052, Optogenetics and Optical Manipulation, 100520J (8 February 2017); https://doi.org/10.1117/12.2249519

[20]. Krassowska, W. (1995), Effects of Electroporation on Transmembrane Potential Induced by Defibrillation Shocks. Pacing and Clinical Electrophysiology, 18: 1644-1660. https://doi.org/10.1111/j.1540-8159.1995.tb06986.x

[21]. DeBruin, K.A., Krassowska, W. Electroporation and Shock-Induced Transmembrane Potential in a Cardiac Fiber During Defibrillation Strength Shocks. Annals of Biomedical Engineering 26, 584–596 (1998). https://doi.org/10.1114/1.101

[22]. Ohuchi K, Fukui Y, Sakuma I, Shibata N, Honjo H, Kodama I. A dynamic action potential model analysis of shock-induced aftereffects in ventricular muscle by reversible breakdown of cell membrane. IEEE Trans Biomed Eng. 2002 Jan;49(1):18-30. doi: 10.1109/10.972836. PMID: 11794768.

[23]. Joshi RP, Mishra A, Hu Q, Schoenbach KH, Pakhomov A. Self-consistent analyses for potential conduction block in nerves by an ultrashort high-intensity electric pulse. Phys Rev E Stat Nonlin Soft Matter Phys. 2007 Jun;75(6 Pt 1):061906. doi: 10.1103/PhysRevE.75.061906. Epub 2007 Jun 7. PMID: 17677299.

[24]. Langus, J., Kranjc, M., Kos, B. et al. Dynamic finite-element model for efficient modelling of electric currents in electroporated tissue. Sci Rep 6, 26409 (2016). https://doi.org/10.1038/srep26409

[25]. D. R. McNeal, “Analysis of a model for excitation of myelinated nerve,” IEEE Transactions on Biomedical Engineering, vol. BME-23, no. 4, pp. 329–337, 1976. doi: 10.1109/TBME.1976.324593.da

[26]. C. C. McIntyre, A. G. Richardson, and W. M. Grill, “Modeling the excitability of mammalian nerve fibers: Influence of afterpotentials on the recovery cycle,” Journal of neurophysiology, vol. 87, no. 2, pp. 995–1006, Feb. 2002, issn: 0022-3077. doi: 10.1152/jn.00353.2001. [Online]. Available: http://intl-jn.physiology.org/cgi/content/full/87/2/995.

[27]. K. W. Altman and R. Plonsey, “Analysis of excitable cell activation: Relative effects of external electrical stimuli,” Medical and Biological Engineering and Computing, vol. 28, pp. 574–580, 2006.

[28]. J. N. Barrett and W. E. Crill, \Specific membrane properties of cat motoneurones," The Journal of Physiology, vol. 239, no. 2, pp. 301{324, jun 1974.
[29]. B. Frankenhaeuser and A. F. Huxley, \The action potential in the myelinated nerve fibre of Xenopus laevis as computed on the basis of voltage clamp data," The Journal of Physiology, vol. 171, no. 2, pp. 302{315, jun 1964.
[30]. C. H. Berthold and M. Rydmark, \Electron microscopic serial section analysis of nodes of Ranvier in lumbosacral spinal roots of the cat: ultrastructural organization of nodal compartments in fibres of different sizes," Journal of Neurocytology, vol. 12, no. 3, pp. 475{505, jun 1983.
[31]. I. Nilsson and C. H. Berthold, \Axon classes and internodal growth in the ventral spinal root L7 of adult and developing cats." Journal of anatomy, vol. 156, no. 2, pp. 71{96, feb 1988.
[32]. M. Rydmark, \Nodal axon diameter correlates linearly with internodal axon diameter in spinal roots of the cat," Neuroscience Letters, vol. 24, no. 3, pp. 247{250, jul 1981.
[33]. Barnett, A. The current-voltage relation of an aqueous pore in a lipid bilayer membrane. Biochim. Biophys. Acta 1025:10–14, 1990.
[34]. Glaser, R. W., S. L. Leikin, L. V. Chernomordik, V. F. Electroporation During Defibrillation Strength Shocks 595 Pastushenko, and A. I. Sokirko. Reversible electrical breakdown of lipid bilayers: Formation and evolution of pores. Biochim. Biophys. Acta 940:275–287, 1988.
[35]. Chernomordik, L. V., S. I. Sukharev, S. V. Popov, V. F. Pastushenko, A. V. Sokirko, I. G. Abidor, and Y. A. Chizmadzhev. The electrical breakdown of cells and lipid membranes: The similarity of phenomenologies. Biochim. Biophys. Acta 902:360–373, 1987.
[36]. Zhou, X., W. M. Smith, D. L. Rollins, and R. E. Ideker. Transmembrane potential changes caused by shocks in guinea pig papillary muscle. Am. J. Physiol. 271:H2536–H2546, 1996.
[37]. Reilly J.P. (1998) Electrical Principles of Nerve and Muscle Function. In: Applied Bioelectricity. Springer, New York, NY. https://doi.org/10.1007/978-1-4612-1664-3_3

SUPPORTING INFORMATION

• List of content

- SI-1. Equations describing the ionic currents 35
- References 37

• SI-1. Equations describing the ionic currents

The equations that describe the ionic currents at the axon's membrane were taken from McIntyre et. al. 2002 [1]. The current in this model were adjusted to represent the excitation of a mammalian motor neuron at 36°C and consist on 3 types of ionic channels and a leakage current [2]. The total ionic current at each node was calculated as the sum of 4 different currents:

$$I_i = I_{Naf} + I_{Nap} + I_{Ks} + I_{Lk} \tag{10}$$

The equations driving the time evolution of these currents and their dependence with the TMV are (expressed in mV and ms):

Fast sodium current

$$I_{Naf} = g_{Naf} m^3 h (V_m - E_{Na}) \tag{11}$$

$$\frac{dm}{dt} = \alpha_m (1 - m) - \beta_m m \tag{12}$$

$$\alpha_m = 6.57 \frac{V_m + 20.4}{1 - \exp[-(V_m + 20.4)/10.3]} \tag{13}$$

$$\beta_m = 0.304 \frac{-(V_m + 25.7)}{1 - \exp[(V_m + 25.7)/9.16]} \tag{14}$$

$$\frac{dh}{dt} = \alpha_h (1 - h) - \beta_h h \tag{15}$$

$$\alpha_h = 0.34 \frac{-(V_m + 114)}{1 - \exp[(V_m + 114)/11]} \tag{16}$$

$$\beta_h = \frac{12.6}{1 + \exp[-(V_m + 31.8)/13.4]} \quad (17)$$

Persistent sodium current

$$I_{Nap} = g_{Nap} p^3 (V_m - E_{Na}) \quad (18)$$

$$\frac{dp}{dt} = \alpha_p (1 - p) - \beta_p p \quad (19)$$

$$\alpha_p = 0.0353 \frac{V_m + 27}{1 - \exp[-(V_m + 27)/10.2]} \quad (20)$$

$$\beta_p = 0.000883 \frac{-(V_m + 34)}{1 - \exp[(V_m + 34)/10]} \quad (21)$$

Slow potassium current

$$I_{Ks} = g_{Ks} s (V_m - E_K) \quad (22)$$

$$\frac{ds}{dt} = \alpha_s (1 - s) - \beta_s s \quad (23)$$

$$\alpha_s = \frac{0.3}{1 + \exp[-(V_m + 53)/5]} \quad (24)$$

$$\beta_s = \frac{0.03}{1 + \exp[-(V_m + 90)/1]} \quad (25)$$

Leakage current

$$I_{Lk} = g_{Lk} (V_m - E_{Lk}) \quad (26)$$

Where g_{Naf}, g_{Nap}, $g_{Ks}$and g_{LK} are the ionic conductances, and E_{Na}, E_k, and E_{LK} are the ionic Nerst potentials. m, h, p and s are the gating variables that modulate the non-linear currents, and α and β are functions of the membrane voltages.

Values of the parameters used to model the ionic currents are: $g_{Naf} = 3\frac{S}{cm^2}$, $g_{Nap} = 0.01\frac{S}{cm^2}$, $g_{Ks} = 0.08\frac{S}{cm^2}$, $g_L = 0.007\frac{S}{cm^2}$, $E_{Na} = 50\,mV$, $E_k = -90\,mV$, $E_L = -90\,mV$ [2].

- **References**

[1]. C.C. McIntyre, A.G. Richardson, W.M. Grill, Modeling the Excitability of Mammalian Nerve Fibers: Influence of Afterpotentials on the Recovery Cycle, J. Neurophysiol. 87 (2002) 995–1006. https://doi.org/10.1152/jn.00353.2001.

[2]. B. Mercadal, C. Arena, R. Davalos, and A. Ivorra, "Avoiding nerve stimulation in irreversible electroporation: A numerical modeling study," Physics in Medicine and Biology, vol. 62, pp. 8060–8079, 2017. doi: https://doi.org/10.1088/1361-6560/aa8c53